MAX-PLANCK-INSTITUT FÜR PLASMAPHYSIK

GARCHING BEI MÜNCHEN

MAGNETIC RECONNECTION

Dieter Biskamp and Helmut Welter

IPP 6/304 October 1991

Abstract

A review is given of the theory of magnetic reconnection in the framework of resistive magnetohydrodynamics (MHD). While most of the material refers to two-dimensional systems, the final sections give a brief outlook of problems arising in fully three-dimensional configurations.

Die nachstehende Arbeit wurde im Rahmen des Vertrages zwischen dem Max-Planck-Institut für Plasmaphysik und der Europäischen Atomgemeinschaft über die Zusammenarbeit auf dem Gebiete der Plasmaphysik durchgeführt.

1 Introduction

There is hardly a term in plasma physics exhibiting more scents, facets and also ambiguities than that of magnetic reconnection or, simply, reconnection. It is even sometimes used with a touch of magic. The basic picture underlying the idea of reconnection is that of two field lines (thin flux tubes, properly speaking) being carried along with the fluid owing to the property of flux conservation until coming close together at some point, where by the effect of finite resistivity they are cut and reconnected in a different way. Though this is a localized process, it may fundamentally change the global field line connection as indicated in Fig. 1, permitting fluid motions which would be inhibited in the absence of such local decoupling of fluid and magnetic field. It has become clear that almost all nonlinear processes in magnetized conducting fluids involve reconnection which may be called the essence of nonlinear MHD.

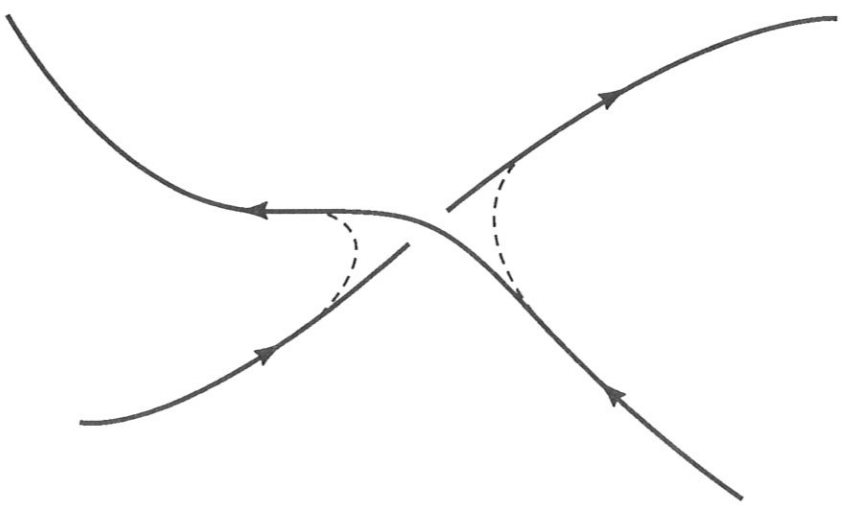

Figure 1: *Change of field line topology due to reconnection.*

Because of the omni-presence of finite resistivity in real systems there is always a certain usually slow rate of resistive diffusion. Reconnection theory is therefore concerned with the problem of *fast reconnection* in order to explain how in certain dynamic processes very small values of the resistivity allow the rapid release of a large amount of free magnetic energy as observed for instance in tokamak disruptions or solar flares. By "fast"we mean faster than the resistive time τ_η associated with the average gradient scale L, $\tau_\eta/\tau_A = S \equiv \eta^{-1}$. Hence a fast process is defined to occur with a time rate $\sim O(\eta^\nu)$ $0 \leq \nu < 1$. (In the literature this attribute is sometimes reserved to the special case $\nu = 0$.)

In section 2 the 2-D resistive MHD equations are introduced which form the usual framework of reconnection theory. Fast reconnection is basically a localized process. The fundamental local reconnecting structure appears to be a current sheet, the basic dynamics of which is introduced in section 3. Conventional reconnection theory is mainly associated with either one of two different lines of thought, Petschek's slow shock model ("X-point"models) and Syrovatskii's current sheet model, which are discussed in section 4. Since these theories deal effectively only with the ideal outer region ignoring the so-called diffusion region, the narrow region where resistivity is important, we call them quasi-ideal models. While Petschek's theory is now known to be incorrect in the limit of small η, providing at most a phenomenological reconnection model in the presence of anomalous, i.e. locally enhanced, resistivity, current sheets by contrast represent a fundamental feature of weakly resistive MHD and Syrovatskii's theory accounts for many properties observed in fully dynamic resistive MHD systems.

In section 5 we summarize the scaling properties of stationary current sheet configurations as observed in numerical simulations.

Section 6 gives a refined theory of dynamical current sheets. We first investigate the properties in the central part, the vicinity of the "X-point", and then discuss the rather complex behavior in the edge region.

The question of tearing instability is a central issue. As numerical simulations indicate, dynamic current sheets are considerably more stable than static sheets, allowing much larger aspect ratio A = sheet width/thickness. A qualitative theory of the stability threshold is given in section 7.

Section 8 presents examples of two-dimensional reconnecting systems, the coalescence of magnetic islands, the nonlinear evolution of the resistive kink

mode, and the process of plasmoid formation.

In section 9 we discuss generalizations of the reconnection concept arising in fully three-dimensional systems.

Finally in section 10 the asymptotic behavior in the large Reynolds number limit is considered, where time dependent, presumably turbulent reconnection processes prevail.

2 The 2-D resistive MHD equations

Theoretical modelling of fast reconnection is mostly confined to 2-D incompressible MHD. In this case the MHD equations

$$\partial_t \mathbf{B} = \nabla \times (\mathbf{v} \times \mathbf{B}) - R_\eta \tag{1}$$

$$\rho\,(\partial_t \mathbf{v} + \mathbf{v} \cdot \nabla \mathbf{v}) = -\nabla p + \mathbf{j} \times \mathbf{B} + R_\mu \tag{2}$$

$$\partial_t \rho + \nabla \cdot \mathbf{v}\rho = 0 \tag{3}$$

$$\text{energy equation for } p \tag{4}$$

can conveniently be written in the form of two scalar equations for a magnetic flux function ψ and a kinetic stream function ϕ eliminating the pressure p and choosing a homogeneous density distribution $\rho = 1$,

$$\partial_t \psi + \mathbf{v} \cdot \nabla \psi = \eta_0 j - \eta_2 \nabla^2 j \tag{5}$$

$$\partial_t \omega + \mathbf{v} \cdot \nabla \omega = \mathbf{B} \cdot \nabla j + \mu \nabla^2 \omega \tag{6}$$

$$\begin{aligned} \mathbf{B}_\perp &= \mathbf{e}_z \times \nabla \psi \quad , \quad \mathbf{v}_\perp = \mathbf{e}_z \times \nabla \psi \\ j &= \nabla^2 \psi \quad , \quad \omega = \nabla^2 \phi \, . \end{aligned}$$

Here the subscript $\perp$ refers to the components perpendicular to the ignorable coordinate z, also called the poloidal components. Note that the parallel or axial components B_z, v_z need not be constant, but their equations decouple from eqs. (5), (6) owing to the incompressibility, hence these quantities could be computed à posteriori. In order to justify the assumption of incompressibility one often invokes the presence of a large axial $B_z = B_0 \gg B_\perp$, such that the poloidal motion becomes essentially an incompressible $\mathbf{E} \times \mathbf{B}$ flow. In this case only the small poloidal field $B_\perp$ is affected by reconnection, which

is true for most laboratory and many astrophysical plasma configurations. It should be noted that the 2-D incompressible eqs. (5), (6) are identical with the 2-D reduced MHD equations (Strauss, 1976).

The 3-D reduced equations are almost identical with the 2-D form,

$$\partial_t \psi + \mathbf{v}_\perp \cdot \nabla \psi = B_0 \, \partial_z \phi = \eta j \tag{7}$$

$$\partial_t \omega + \mathbf{v}_\perp \cdot \nabla \omega = B_\perp \cdot \nabla j + B_0 \, \partial_z j + \mu \nabla_\perp^2 \omega \tag{8}$$

the only coupling terms in the z-direction being provided by the linear terms $\propto B_0$.

The dissipative terms as written in eq. (5) contain a scalar resistivity η_1, usually denoted simply by η, and a hyperresistivity, representing an anomalous electron viscosity. While most of the discussion will be confined to the case of a homogeneously distributed scalar resistivity, we also consider the effect of hyperresistivity which may become the dominating magnetic dissipation process in certain weakly collisional plasmas. Viscous dissipation is confined to a simple scalar viscosity μ, which is not a very restricting assumption, since the reconnection process is primarily determined by magnetic dissipation, except for very large viscosity.

Equations (5), (6) are written in nondimensional form normalizing $B_\perp$ to some typical poloidal field $B_{\perp 0}$, $v_\perp$ to the corresponding Alfvén speed $v_A = B_{\perp 0}$ since $\rho = 1$, and spatial coordinates to some typical scale L. Hence the dimensionless parameter η is $\eta / L v_A = S^{-1}$, the inverse Lundquist number and correspondingly for η_2 and μ.

3 Current sheets : Basic properties

3.1 Sweet-Parker current sheet model

If fluid volumes carrying oppositely directed magnetic fields are pushed toward each other, the fluid is squeezed sidewise along the field and the fields approach each other, until resistive diffusion becomes important. The result is a quasi-stationary dynamic current sheet, called Sweet-Parker current sheet (Sweet, 1958; Parker, 1963), which is the simplest reconnection configuration illustrated in Fig. 2. As usual we assume incompressible motions with homogeneous mass density, $\rho = 1$. The quasi-one-dimensional configuration is characterized by six parameters, three dynamic quantities : the magnetic field B_0 immediately outside the sheet called the upstream field (the downstream

field at the sheet edges is small in this quasi-one-dimensional configuration), the upstream flow u_0 perpendicular to the field and the downstream flow v_0 along the field; two geometric quantities : the width Δ (implying that the sheet length is measured in the third direction z) and the thickness δ, and finally the resistivity η.

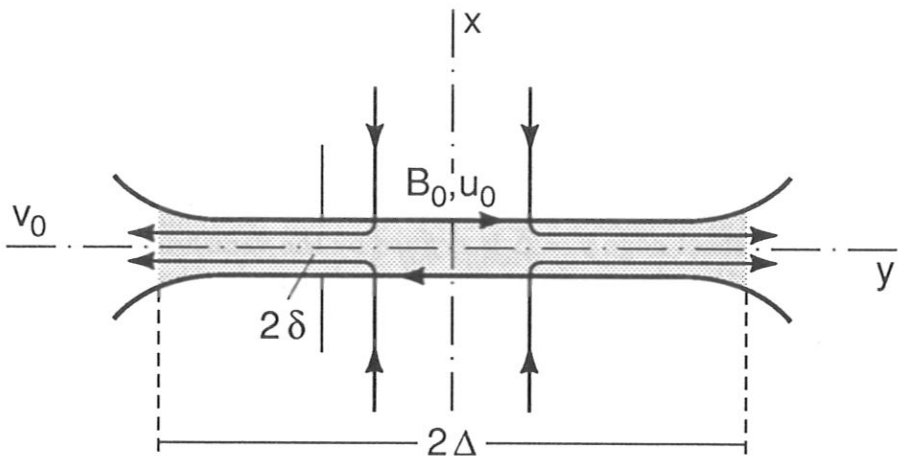

Figure 2: *Dynamic (Sweet-Parker) current sheet.*

These quantities are connected by three relations derived from the continuity equation, Ohm's law, and the equation of motion assuming stationarity. Integrating the continuity equation $\nabla \cdot \rho \mathbf{v} = 0$ over the inflow and outflow surfaces gives

$$u_0 \Delta = v_0 \delta \,. \tag{9}$$

Consider Ohm's law along the x-axis. Stationarity requires $E_z = const.$ In the upstream region outside the sheet, where the current density is small, the resistive term in Ohm's law is negligible, while in the current sheet center

where $j = j_m$ is large and the velocity vanishes and thus the resistive term dominates, which gives the relation

$$u_0 B_0 = \eta j_m \simeq \eta \frac{B_0}{\delta} . \tag{10}$$

Since usually $u_0 \ll B_0$ as will be seen à posteriori, the inertia term is negligible in the force balance across the sheet. Hence $\partial_x (p + B^2/2) = 0$, which gives

$$B_0^2/2 = p_m - p_0 . \tag{11}$$

Here p_0 is the upstream fluid pressure and p_m the maximum pressure in the sheet center, where the magnetic field vanishes. Now consider the force balance along the sheet-midplane. Since B_x is negligible, the magnetic force vanishes, such that only the pressure force is present leading to fluid acceleration along the sheet $v_y \partial_y v_y = -\partial_y p$. Integration between center and edge yields

$$v_0^2/2 = p_m - p_0 . \tag{12}$$

Here the current sheet edge $y = \Delta$ is *defined* by the vanishing of the pressure difference across the sheet. In reality the edge region has a complicated structure, as will be shown in section 5, where a more quantitative description of a current sheet is presented. Substituting $p_m - p_0$ by $B_0^2/2$ we obtain the important result that the downstream flow velocity equals the upstream Alfvén speed

$$v_0 = B_0 = v_A \tag{13}$$

because of the density normalization. Relations (9) and (10) can now be used to express two of the remaining variables by the three other. Choosing the latter as B_0, Δ, η one obtains

$$\frac{u_0}{v_A} \equiv M_0 = \left(\frac{\eta}{B_0 \Delta} \right)^{1/2} \equiv S_0^{-1/2} \tag{14}$$

$$\frac{\delta}{\Delta} \equiv A^{-1} = S_0^{-1/2} . \tag{15}$$

Here we have introduced the Mach-number M_0, which is conventionally used as a dimensionless measure of the reconnection rate implying steady state conditions at least locally in the sheet such that $M_0 \propto \eta j_m$*). A is called the

*)Calling $M = u/B$ the reconnection rate has led to some confusion, since properly speaking the reconnection rate is the rate of flux change at the X-point, $\partial_t \psi_x = \eta j_x$, which equals the product uB for stationary conditions.

aspect ratio and S_0 is the Lundquist number of the current sheet. The Sweet-Parker reconnection rate $M_0 = S_0^{-1/2}$ is a characteristic quantity for a current sheet. If B_0 and Δ are of the order of the global field intensity and spatial scale of the magnetic configuration, S_0 is the global Lundquist number, which in most cases of practical interest is very large, typically 10^{10} in the solar corona, such that the Sweet-Parker rate would lead to reconnection times in a solar flare many orders of magnitude larger than observed. Obviously a single quasi-stationary current sheet of an aspect ratio $A \sim 10^5$ is a very implausible configuration.

It was in fact in flare theory where the need for a faster reconnection process became first evident. Here Petschek's slow shock mechanism (Petschek, 1964) seemed to provide a simple and elegant solution. This configuration, too, contains a current sheet, where reconnection occurs, but its width Δ is not determined by the overall system size but forced by the configuration to be very small $\Delta \sim O(\eta)$. Hence the reconnection rate becomes essentially independent of the resistivity which is what observations seem to demand. Unfortunately, however, Petschek's model incorporates a fundamental inconsistency invalidating the theory in the most interesting regime of small resistivity as discussed in section 4.2. Instead it is found that in an intermediate resistivity regime reconnection occurs in fact in macroscopic current sheets, in the original sense of the Sweet-Parker reconnection model, while for smaller resistivities the reconnection process becomes instationary, leading to fully developed turbulence in the limit of $\eta \to 0$.

Current sheets are formed under quite general conditions. In particular the field must not be strictly anti-parallel, vanishing at the neutral line, but only a particular component, called the poloidal field, has to change sign. Hence there is in general a finite axial field B_z in the sheet region. Where in a sheared magnetic configuration a current forms, depends on the flows as excited for instance by an MHD instability. Several examples will be presented in section 8.

A strong axial field $B_z \gg B_y \sim B_0$ provides also a solid justification of the incompressibility assumption, which might otherwise appear doubtful within the sheet, where the fluid velocity becomes large. The criterion for incompressible motion is $v_{\|} \ll c_s$ for parallel flow and $v_{\perp} \ll v_A$ for perpendicular flow. In the absence of an axial field incompressibility is valid only for the case of high β, where $p_0 \gg B_0^2/2$, such that $p_m - p_0 \ll p_0$. High-β plasmas, which can only be confined by gravitation, are however not very interesting,

since the typical plasma properties result from the interaction with magnetic fields. By contrast a strong axial component corresponding to the case of magnetically confined plasma with relatively low β, automatically guarantees incompressibility. Even if the flow reaches the Alfvén speed, meaning the poloidal Alfvén speed, eq. (13), it is still slow compared with the axial one, and hence constitutes essentially an incompressible $\mathbf{E} \times \mathbf{B}$ convection.

3.2 Effect of hyperresistivity and viscosity

Besides resistivity further dissipation processes may be important, changing the current sheet scaling laws. Let us first consider hyperresistivity η_2, introduced in eq. (5). Equation (10) is replaced by

$$u_0 B_0 = \eta_2 \, \partial_x^2 j_m \simeq \eta_2 \frac{B_0}{\delta^3} \tag{16}$$

while the force balance and hence the relation $v_0 = B_0$ remain unchanged. Insertion into the mass conservation relation (9) gives the Mach number

$$M = \left(\frac{\eta_2}{B_0 \Delta^3} \right)^{1/4} . \tag{17}$$

Hence the η_2-dependence of M is weaker than that on $\eta = \eta_1$, eq. (14), making the reconnection time scale less sensitive to the actual value of the transport coefficient.

Also fluid viscosity μ, corresponding to ion viscosity in a plasma, could be an important effect, modelling for instance dissipation due to gyro-resonance in an nearly collisionless plasma. The case of finite viscosity has been considered by Park et al. (1984). The parallel force balance along the sheet now becomes $v_y \partial_y v_y - \mu \partial_x^2 v_y = -\partial_y p$, since $\nabla^2 v_y \simeq \partial_x^2 v_y$. Integrating between center and edge of the sheet, using $\int_0^\Delta \partial_x^2 v_y dy \simeq -v_0 \Delta / 2\delta^2$ and eq. (11), one obtains

$$v_0^2 + \left(\mu \Delta / \delta^2 \right) v_0 = B_0^2$$

or, with $v_0 = \eta \Delta / \delta^2$ from eqs. (9), (10),

$$v_0 = B_0 \left(1 + \frac{\mu}{\eta} \right)^{-1/2} \tag{18}$$

and hence

$$M = S_0^{-1/2}\left(1+\frac{\mu}{\eta}\right)^{-1/4} \tag{19}$$

$$A = S_0^{1/2}\left(1+\frac{\mu}{\eta}\right)^{-1/4}, \tag{20}$$

generalizing eqs. (14) and (15). Thus the modifications introduced by viscosity are relatively mild. While for $\mu \lesssim \eta$ its effect is negligible, $\mu \gg \eta$ results in a broader sheet with reduced inflow and outflow velocities.

4 Quasi-ideal models of stationary reconnection

4.1 Driven reconnection

The concept of driven reconnection plays an important role in conventional reconnection theory. Originally the term refers to externally forced systems in contrast to closed systems where internal reconnection processes occur spontaneously for instance as a result of some instability. The concept can, however, be applied much more generally. If we assume that the process of reconnection is localized in space, we may restrict consideration to a small region of linear dimensions L around this location instead of the entire system, open or closed, of scale size Λ, $L \ll \Lambda$. On the other hand L should be large compared to the scales of the dissipative structures, $L \gg \Delta$ in the case of a single current sheet, so that these are not affected by the artificial boundaries of the subsystem. The main advantages of restricting attention to the subsystem L are that it allows to simplify the geometry and also to assume stationarity even for a nonstationary global system. Since the coupling to the latter occurs by the boundary conditions imposed on the subsystem, and these boundary conditions change on the global time scale $\sim \Lambda/v_A$, while the subsystem adjusts to these changes on the much faster time scale $\sim L/v_A$, we may consider the latter in steady state (if such state exists).

In this sense the subsystem constitutes a stationary reconnection configuration. As for instance shown in Figs. 3 and 5, fluid and magnetic field are injected from above and below, while the fluid leaves the system laterally carrying along the reconnected field. The small region, where dissipation processes, in particular resistivity, are important, is called the *diffusion region*,

which is surrounded by the *ideal external region*, where dissipation effects are negligible. The interpretation of such a model system has, however, given rise to some confusion. Since the fundamental issue in reconnection theory is to account for rapid processes, a particular figure of merit of a theoretical configuration is a weak or possibly no dependence of the reconnection rate on the resistivity. In stationary driven reconnection this point needs further specification, since the reconnection rate is determined by the boundary conditions for the inflow velocity and magnetic field intensity and thus independent of η per definition. Instead for the reconnection process to be independent of η one has to require that at fixed boundary conditions the *configuration* remains unchanged if η is varied, at least for sufficiently small values of η. A consequence of such behavior would be that the ratio of outflow energy flux to input energy flux should be independent of η (essentially unity) and so should be the ratio of the energy dissipation rate and the input energy flux (essentially zero).

4.2 Petschek's slow shock model

The model proposed by Petschek 1964 at a symposium on solar flares was almost immediately accepted as a major breakthrough in the theory of reconnection, serving as the basic concept for the following two decades. In fact most papers (at least in the western hemisphere) on the subject of reconnection deal with one or the other variant of Petschek's model, notably the review article by Vasyliunas (1975), or a subsequent review by Forbes and Priest (1987). Only in recent years the basic inconsistency in the theory has become apparent. Because of its historical importance Petschek's model shall be briefly described, before we point out where the theory is in error, both conceptionally and formally.

The configuration is illustrated in Fig. 3. It is characterized by two pairs of slow mode shocks standing back to back against the upstream flow, deviating it by roughly 90^0 into the downstream cone, where the magnetic field is weak. The current and vorticity are concentrated in the shock fronts and the central diffusion layer, while in the external region velocity and magnetic field are irrotational, $\nabla \times \mathbf{v} = \nabla \times \mathbf{B} = 0$, which together with $\nabla \cdot \mathbf{v} = \nabla \cdot \mathbf{B} = 0$ results in $\nabla^2\psi = \nabla^2\phi = 0$. The shocks derive their properties from the slow magnetosonic mode. This is primarily a longitudinal compressible mode, which at finite amplitude steepens to form a shock. Its pecularity is to survive with finite phase velocity in the incompressible limit, $\omega^2 = k_\parallel^2 v_A^2 = k^2 B_n^2$, where B_n is the component normal to the wave front. Hence for a given flow

speed a plasma flow can always become supersonic with respect to this mode if the angle between wave front and magnetic field is made sufficiently small.

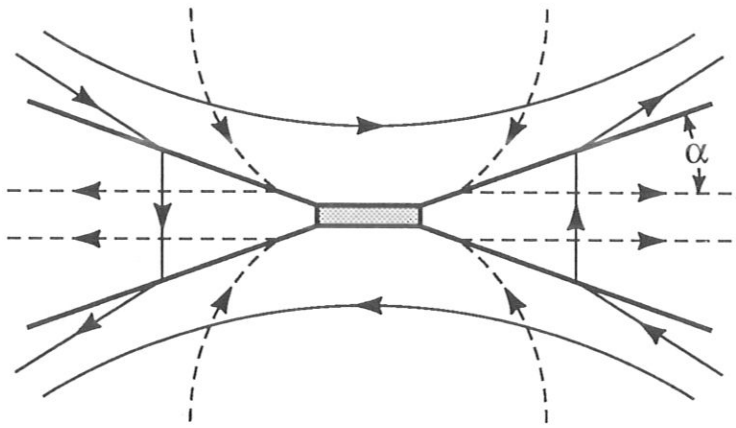

Figure 3: *Schematic drawing of Petschek's reconnection configuration.*

The jump conditions across a slow mode shock in the incompressible limit can easily be derived. Equations $\nabla \cdot \mathbf{v} = \nabla \cdot \mathbf{B} = 0$ give

$$[v_n] = [B_n] = 0\,, \tag{21}$$

where $[f]$ indicates the change across the shock. From the normal component of the equation of motion follows the continuity of the total pressure

$$\left[p + B^2/2\right] = 0\,, \tag{22}$$

while from the tangential component follows

$$[v_t] = [B_t]\,. \tag{23}$$

Using this result in Ohm's law for steady state $\mathbf{v} \times \mathbf{B} = const$ yields

$$v_n = B_n \,. \tag{24}$$

If we require that for a given upstream magnetic field $\mathbf{B}^{(1)}$ the velocity and the magnetic field in the downstream cone are homogeneous as indicated in Fig. 4, $v_x^{(2)} = B_y^{(2)} = 0$, the angles α, β are determined as well as the tangential component $v_t^{(1)}$ of the upstream velocity. For small Mach number $v^{(1)}/B^{(1)} \ll 1$ the downstream cone is narrow $\alpha \ll 1$, $\beta = \alpha$, and $v^{(2)} = B^{(1)}$, the upstream Alfvén speed.

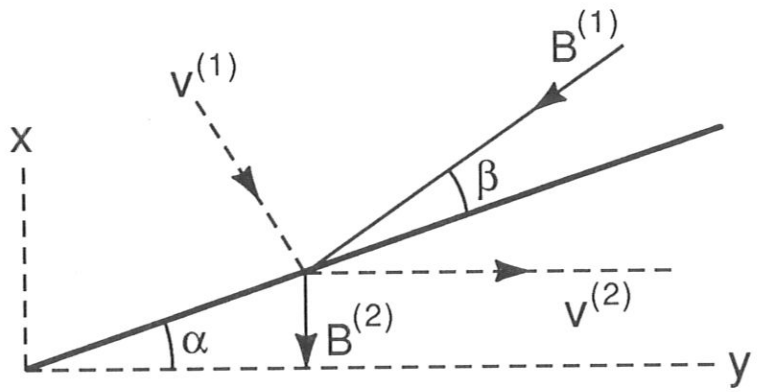

Figure 4: *Illustration of* $\mathbf{B}$ *and* $\mathbf{v}$ *at the Petschek slow shock (heavy line) and definition of angles* α *(downstream cone) and* β, $B_n = B \sin \beta$.

The crucial (and basically wrong, as we shall see) assumption in Petschek's model is, that the diffusion region is small, a tiny current sheet of dimensions $\Delta \sim \delta \sim \eta$, adjusting smoothly to the external configuration, where the latter is completely determined by the outer boundary conditions. (If this were true, then by the definition given in section 4.1 the reconnection rate would in fact be independent of η.) To determine the ideal external configuration the equations $\nabla^2 \psi = 0$, $\nabla^2 \phi = 0$ are solved in the limit $\Delta \to 0$ using the jump conditions at the shock. Petschek gives an analytical solution in the

limit $M \ll 1$. Since the downstream flow equals the upstream Alfvén speed, it follows from mass conservation that $M \simeq \alpha$, the angle of the downstream cone. Petschek obtains the maximum reconnection rate achievable in his model

$$M_{max} \simeq \left(\ln \frac{L}{\Delta}\right)^{-1} \simeq (\ln S)^{-1} \ . \tag{25}$$

This weak S- or η-dependence is simply due to the fact that the magnetic field is weaker in front of the diffusion layer than the asymptotic field, assumed to be homogeneous, which is used in the definition of M in eq. (25).

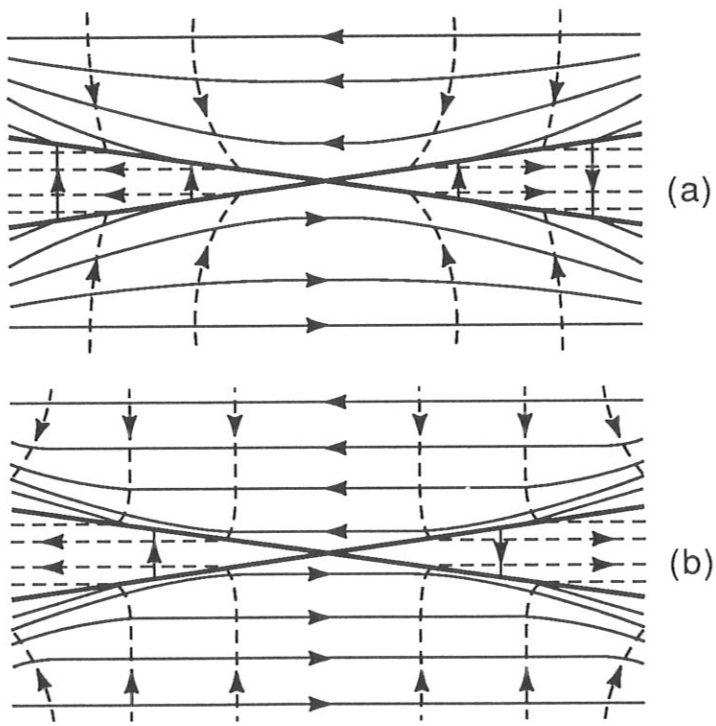

Figure 5: *Petschek-type reconnection configurations:*
magnetic field lines (full), stream lines(dashed), slow mode shocks (heavy).
(a) Petschek's original configuration ("fast mode expansion").
(b) Sonnerup-type configuration ("slow mode expansion").

More general solutions are obtained by relaxing the condition of irrotational $\mathbf{v}$ and $\mathbf{B}$, which allows for instance configurations with constant upstream magnetic field as shown in Fig. 5b with $M_{max} = O(1)$ independent of η. Special similarity solutions of this type have been given by Sonnerup (1970) and Yeh and Axford (1970) consisting of three regions (per quadrant) of homogeneous velocity and magnetic field, separated by two singular lines, the Petschek shock and a second line in the upstream region, in which the current and vorticity of the upstream region are concentrated. A wider class of analytical solutions containing Petschek's and Sonnerup's as special case has been given by Priest and Forbes (1986).

By calling all these configurations, which are usually strictly distinguished in the literature, Petschek-like, it is indicated that their differences are minor compared with the common basic assumption concerning the effect of the diffusion region. In fact all are solutions of the ideal external region which essentially ignore the dynamics in the diffusion region, whence the term quasi-ideal reconnection models. It is true that Petschek includes a treatment of the diffusion layer, which, however, can only be regarded as an interpolation between the origin and the external solution, assuming, for instance, a linear increase of the perpendicular field component $B_x \propto y$, while a rigorous treatment shows $B_x \propto y^3$ as will be discussed in section 5.1.

Petschek's model is based on the analog of a system of two supersonic gas streams hitting head-on and being deflected sidewise by shocks with the same geometry as the Petschek shocks. The physics of the central stagnation point, where the shocks join, is however quite different in both cases. While it is an ordinary flow stagnation point in the case of a nonmagnetic neutral fluid, it is the location of intense dissipation and magnetic diffusion, owing to high current density in the case of a magnetized conducting fluid. In the latter case the flow is only supersonic with respect to the slow mode, while it is subsonic with respect to the magneto-sonic mode, the phase velocity of which is in fact infinite in the incompressible approximation. If resistive diffusion is reduced by decreasing η, the field is locally compressed in front of the diffusion layer, which effect is communicated upstream modifying the entire upstream configuration, in contrast to a supersonic gas stream, where no signal can propagate upstream.

In fact from a plasma physics point of view Petschek's concept contradicts intuition, which tells us that pushing two volumes of highly conducting plasma with opposite magnetic fields toward each other produces a flat configuration with a current sheet and that pushing faster makes the configuration

more flattish instead of further opening-up the cone for sidewise ejection, $M = \alpha$, as predicted in a Petschek-like model. Intuition is corroborated by numerous numerical simulations, all exhibiting formation of current sheets for sufficiently small η, becoming longer, if η is reduced instead of shorter. Scaling laws of current sheet configurations are discussed in section 5.

The crucial deficiency of reconnection models of the Petschek-type is the ignorance or inappropriate treatment of the diffusion region. A correct theory requires the solution of the boundary layer problem, matching the inner resistive solution computed in simplified geometry to the external ideal solution. Petschek's external solution is correct and even stable, but it does not match to the diffusion layer for small η. Eliminating the problem of the diffusion layer by using a resistivity profile which is locally strong enhanced in the vicinity of the X-point, $\eta_X = O(1)$ ("anomalous resistivity"), a Petschek-like configuration is in fact set up as seen in the simulations by Sato and Hayashi (1979). Hence Petschek's model is not a selfconsistent reconnection model in the limit of small η. Because of the complexity of the diffusion layer, which will be discussed in section 6, it appears quite hopeless to solve the matching problem analytically. Quasi-exact stationary solutions for relevantly small values of η have, however, been obtained by numerical simulation (e.g. Biskamp, 1986), which are presented in sections 5 and 6. All these configurations are strongly dependent on η and become nonstationary, if η falls below some threshold.

The fact that numerical simulations of driven reconnection do not reproduce a Petschek-like configuration for small η, has sometimes been attributed to an inappropriate choice of the boundary conditions. While the discussion of boundary conditions, in particular the actual freedom in their choice, is deferred to section 5, we here only point out that the simulations themselves effectively invalidate this argument.

a) Various kinds boundary conditions have been used in driven reconnection simulations, none of which lead to a Petschek-type configuration for small η. However, allowing anomalous resistivity to eliminate the diffusion layer problem, Petschek-type configurations are set up for the same boundary conditions.

b) Various simulations of self-consistent reconnecting systems have been performed, such as the process of island coalescence (section 8.1) or the nonlinear resistive kink mode (section 8.2), where no internal boundary conditions that could possibly infer with the reconnection process have to be imposed. All develop extended current sheets for small η.

4.3 Syrovatskii's current sheet solution

An alternative school of thought, with adherents mainly in the eastern hemisphere, originated from Syrovatskii's theory of current sheet formation (Syrovatskii, 1971). Similarly to Petschek's model this is also a quasi-ideal, quasi-stationary approach, dealing only with the ideal solution, which may, however, exhibit sheet-like singularities. Though Syrovatskii's theory does not describe real configurations with high reconnection rates in the limit of small η, it provides a qualitatively correct picture for not too strong external driving.

The basic equations are somewhat different from those of two-dimensional incompressible MHD, to which the major part of this chapter is confined, using vanishing plasma pressure $p = 0$ instead. The main assumption is that all currents in the system are localized in isolated current sheets. Hence ψ satisfies Laplace's equation

$$\nabla^2 \psi = 0 \,, \tag{26}$$

such that ψ is a harmonic function and one can use complex analysis. The solution is determined by the boundary conditions. If these change in time, ψ obtains a parametric time dependence $\psi\,(x, y, t)$, which then determines the perpendicular component $\mathbf{v}_\perp$ of the velocity from the frozen-in condition,

$$\begin{aligned} \frac{d\psi}{dt} &\equiv \partial_t \psi + \mathbf{v} \cdot \nabla \psi = 0 \\ \mathbf{v}_\perp = -\partial_t \psi \nabla \psi / |\nabla \psi|^2 \,&, \; \mathbf{B} = \mathbf{e}_z \times \nabla \psi \,, \end{aligned} \tag{27}$$

while the parallel component $\mathbf{v}_{||}$ is calculated from the equation

$$\begin{aligned} \frac{d\mathbf{v}}{dt} \times \nabla \psi &= 0 \\ \mathbf{v}_{||} &= \mathbf{v} - \mathbf{v}_\perp \,, \end{aligned} \tag{28}$$

which follows from the equation of motion using $p = 0$. (The latter equation, however, implies that the current density and hence the Lorentz force does not vanish identically. Hence eq. (26) has to be regarded as an approximation in the sense that the effect of the distributed currents is small compared to that of the sheet current.) The flow is in general not incompressible. We should, however, note that $\mathbf{v}$ is determined à posteriori, which seems to reduce the theory to eq. (26), i.e. an equilibrium boundary value problem. The important point is, that smooth solutions do in general not exist, in the sense that any change of the boundary conditions leading to a change of ψ, $\partial\psi/\partial t \neq 0$, at a neutral point $\nabla\psi = 0$ gives rise to a singular current.

To discuss this singularity in more detail it is convenient to introduce the complex potential $F(z)$ in the complex plane $z = x + iy$,

$$F(z,t) = \psi(x,y,t) + i\chi(x,y,t)\,, \tag{29}$$

which is analytic in the region considered except for isolated singular points and branch cuts. The conjugate harmonic function χ can be determined by using the Cauchy-Riemann relations

$$\partial_x\chi = -\partial_y\psi\ ,\ \partial_y\chi = \partial_x\psi\,. \tag{30}$$

From eq. (29) we obtain the magnetic field in the form

$$dF/dz = B_y + iB_x\,, \tag{31}$$

which can be seen by choosing a special direction of the derivative, e.g. dF/dx, since owing to eqs. (30) the complex derivative is independent of this choice.

Let $z = 0$ be the position of a neutral point of the magnetic configuration at time $t = 0$, $dF/dz|_{z=0} = 0$. In the vicinity of this point the complex potential is

$$F(z,t) = \frac{\alpha(t)}{2}z^2 + \beta(t)\,, \tag{32}$$

restricting consideration to the only practically relevant case of second order neutral points. Note that owing to eq. (26) there are only X-type nonsingular neutral points. If the change of the boundary conditions for ψ is such that $d\beta/dt \neq 0$, this implies a nonvanishing electric field $E_z = \partial\psi/\partial t$ at the neutral point indicating that the potential $F(z,t)$ cannot remain analytic in the vicinity of the neutral point.

The most natural assumption, namely the induction of a line current at the neutral point,

$$F(z,t) = \frac{\alpha(t)}{2}z^2 + \beta(t) + \frac{I(t)}{2\pi}\ln z\,, \tag{33}$$

is not allowed, since this would give rise to the appearance of an O-type singular neutral point, Fig. 6, implying a change of magnetic topology in a finite region, which is prohibited by condition (27). Here $I(t)$ is the total current generated in the plasma, which is determined by the boundary conditions with

the initial condition $I(0) = 0$.

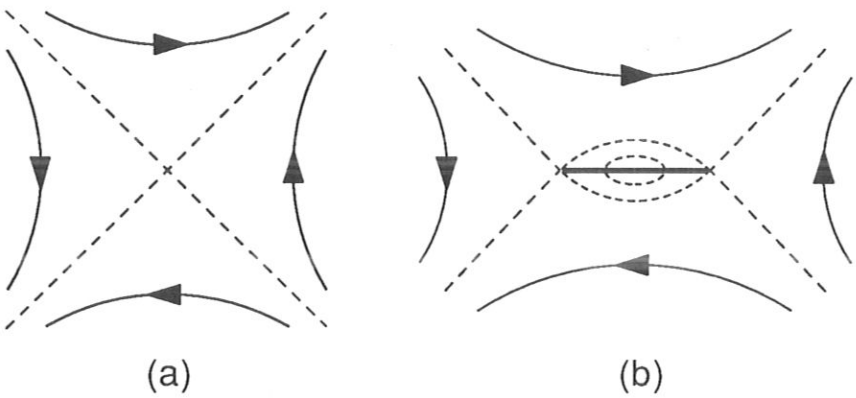

Figure 6: *Generation of a singular current at an X-point. (a) Initial non-singular configuration; (b) effect of an induced singular line current in the original X-point, leading to a fictitious O-point and two adjacent X-points. The heavy line indicates the actually arising sheet current.*

The only admissible alternative is a solution with a branch cut corresponding to a current sheet. The location of a branch cut is determined by that of the fictitious neutral points arising by the addition of a line current in the original X-point. As indicated in Fig. 6b, the cut passes through this point and the two adjacent X-points drifting away from each other as the current $I(t)$ increases.

We can now discuss the structure of the field in the vicinity of a current sheet. At large distances from the region of the cut the potential $F(z,t)$ has approximately the form (33). The conditions at the cut are, that $\mathbf{B}$ does not intersect the cut, since field lines remain continuous if they are so initially. Hence the cut is a line $\psi = const.$ Assume a straight cut extending along the y-axis between the points $y = \pm b$. The solution for the complex potential with the asymptotic form (33) for $|z|/b \gg 1$ and $\psi = 0$ at the cut is given by

$$F(z) = \frac{\alpha}{2} z\sqrt{z^2 + b^2} + \frac{I}{2\pi} \ln \frac{z + \sqrt{z^2 + b^2}}{b} \tag{34}$$

with the derivative

$$\frac{dF}{dz} = B_y + iB_x = \frac{\frac{I}{2\pi} + \alpha\frac{b^2}{2} + \alpha z^2}{\sqrt{z^2 + b^2}}. \tag{35}$$

While the magnetic potential $\psi(x,y) = Re\{F(z)\}$ is continuous, the magnetic field B_y has a jump across the cut, the line density of the current carried by the sheet

$$J(y) \equiv B_y(0_+, y) - B_y(0_-, y) = 2\left(\frac{I}{2\pi} + \alpha\frac{b^2}{2} - \alpha y^2\right) \Big/ \sqrt{b^2 - y^2} \tag{36}$$

with

$$\int_{-b}^{b} J(y)\, dy = I\,.$$

The current distribution (36) shows an interesting feature. It is positive, i.e. in the direction of the total current I, in the center part $|y| < y_0$ and negative, i.e. in the opposite direction, in the outer parts $|y| > y_0$, where $y_0^2 = (I/2\pi\alpha) + b^2/2$. The points $z_\pm = (0, \pm y_0)$ are neutral points of the magnetic field, $dF/dz = 0$, where the separatrix branches off the y-axis, while the current sheet continues along the y-axis, Fig. 7a. At the end points $|y| = b$ the current density $J(y)$ becomes singular giving rise to infinitely large magnetic fields. Only in the special case $I = \pi\alpha b^2$, where the neutral points coincide with the current sheet endpoints the singularity vanishes, Fig. 7b. This value is in fact an upper limit of the current I (or a lower limit of the sheet width b), since for larger values the points $z_\pm$ would form isolated neutral points – the separatrix would be similar to the dashed line drawn in Fig. 6b – which because of the frozen-in property is topologically not possible. The general features of the Syrovatskii current sheet, eq. (36), agree well with those of dynamic current sheets in a fully resistive theory (section 6).

The velocity field $\mathbf{v}$ corresponding to the magnetic configuration (35), which is determined by eqs. (27), (28), cannot be given, as it seems, in simple analytical form, but must be computed numerically, even in the stationary case $\partial_t\psi = const.$ The qualitative behavior close to the current sheet can, however, easily be understood. It follows from eq. (27) that there is a net plasma flux into the sheet $v_x(0_+, y) = -v_x(0_-, y) \neq 0$. Mass conservation then requires the plasma to flow along the sheet, which leaves the sheet at high speed close to the neutral points $z_\pm$, while the plasma flow vanishes at

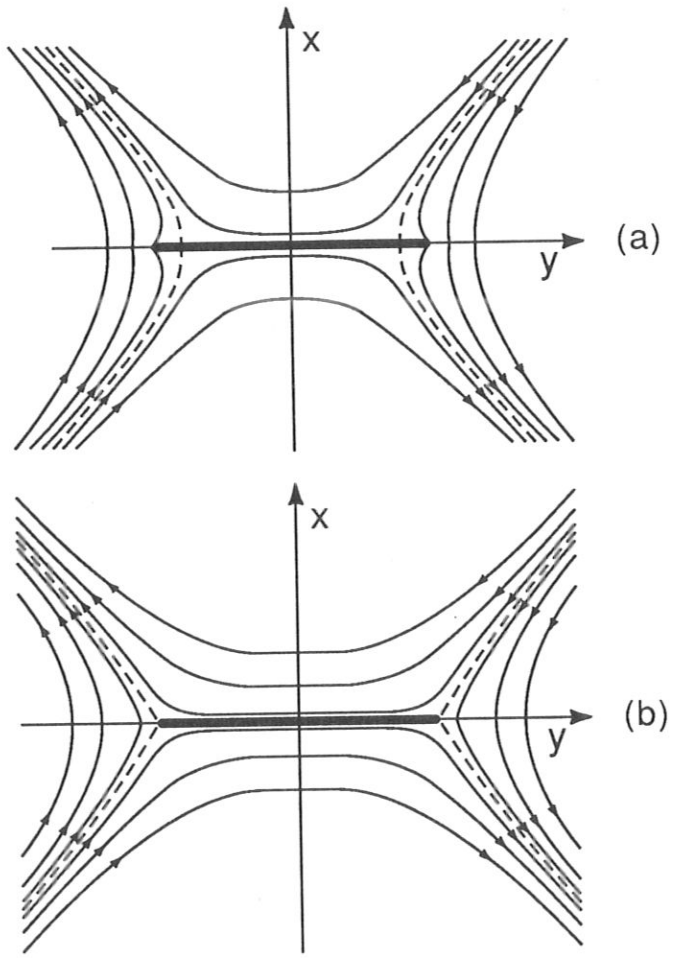

Figure 7: *Contours of the magnetic potential $\psi = Re\{F\}$, where F is given by eq.(34); heavy line = current sheet, dashed line = separatrix. (a) general case $y_0 < b$ exhibiting singularities at the current sheet endpoints; (b) limiting regular case $y_0 = b$ (from Syrovatskii, 1971).*

the singular sheet ends. The downstream velocity in the cone formed by the two branches of the separatrix is of the order of the upstream flow, the cone angle is not related to the downstream flow speed. Evidently Syrovatskii's configuration is basically different from Petschek's.

Syrovatskii's approach is a quasi-static model and does not provide a selfconsistent dynamic model. The configuration is independent of the reconnection rate $\partial_t \psi$, which is an independent parameter in the theory, while a fully resistive theory predicts a strong coupling between the current sheet width b, the reconnection rate and the value of the resistivity. But the qualitative features of the configuration are in surprisingly good agreement with typical current sheet configurations obtained from resistive theory. The essential merit of Syrovatskii's theory is to give a simple and elegant model accounting for the generation of current sheets, a process, which seems to be the most fundamental dynamical feature in highly conducting magnetized fluids.

5 Scaling laws in stationary current sheet reconnection

In order to determine the η-dependence of a stationary driven reconnection configuration the stationary resistive MHD equations must be solved for given inflow and outflow boundary conditions. Unfortunately it appears that the problem is too complicated to permit analytical solutions without severe approximations. In particular the matching of the solution in the diffusion layer to that in the ideal external region is virtually impossible, since the complicated shape of the diffusion region (section 6) seems to make the problem nonseparable, i.e. truly two-dimensional.

Hence we have to resort to numerical methods. In this case there is no particular advantage to restrict consideration to the stationary problem. In fact the simplest and most reliable way is to follow the system numerically from an initial state for fixed boundary conditions, until a stationary state is reached, which automatically eliminates unstable solutions. In the past the objections against a purely numerical way of solution have been, that the limited spatial resolution would not allow to obtain solutions in the interesting range of small η, where small scale structures are expected, and even if we had such solution it would correspond only to one point in parameter space and one would not know how it changes if parameters are varied. For the

problem of two-dimensional stationary driven reconnection these objections are no longer valid. Accurate numerical solutions in the relevant parameter regime can now be obtained and since there are only two essential parameters their scaling laws can be obtained from a rather small number of computer runs.

Since primary interest is in understanding the qualitative behavior one can choose the simplest possible geometry having up-down and right-left symmetry, such that only a quadrant must actually be computed. The computational system is indicated in Fig. 8. The basic equations to be solved are the 2-D incompressible MHD equations (5), (6). Boundary conditions have to be assigned to ψ, ϕ, j, ω. While at the internal boundaries, the x-axis and the y-axis, boundary conditions follow from the imposed symmetry, ψ, j being symmetric, ϕ, ω antimetric, conditions at the upper ($x = L_x$) and the left-hand ($y = L_y$) boundaries correspond to the inflow and outflow conditions, respectively. These should be chosen in a way conforming with the concept of an open system, such that boundaries, in particular the outflow boundary, do not obstruct the flow. Open boundaries are well defined for linear waves requiring that waves are not reflected at the boundary, or, in mathematical terms, that for a hyperbolic system of differential equations all characteristics should be outgoing at the boundary, which guarantees that perturbations arising due to presence of the boundary do not propagate into the system. However, equations (5), (6) of incompressible dissipative MHD are of mixed hyperbolic-parabolic type. In addition the equations are nonlinear and two-dimensional, and to date there is no rigorous method to determine, whether for such system a particular set of boundary conditions is admissible. (A detailed discussion of the boundary conditions for different MHD systems has been given by Forbes and Priest, 1987.)

Let us therefore apply a more practical procedure. While it seems to be sufficient to require continuity of ω and j at the boundaries in eq. (6), $\partial_n \omega = \partial_n j = 0$, the system is more sensitive to the boundary conditions for the potentials ψ in eq. (5) and ϕ in the Poisson equation $\nabla^2 \phi = \omega$, since an inappropriate choice may lead to singularities in ω, j, which would show up in the form of slow shocks in the vicinity of the boundaries. Any choice of the boundary conditions that does not give rise to such singularities should be regarded as acceptable and numerical experience indicates that there is considerable freedom in this choice (Biskamp, 1986). One may, for instance, specify $\phi(y)$ and $\partial_x \psi$, i.e. $v_x(y)$ and $B_y(y)$ at the ingoing boundary $x = L_x$ and $\phi(x)$, i.e. $v_y(x)$, at the outgoing boundary $y = L_y$ and iterate $\partial_y \psi$, i.e.

$B_x(x)$, at the latter, until the outflow configuration becomes smooth.

In order to describe the dependence of the configuration on the inflow conditions it is convenient to parametrize the inflow boundary functions writing $v_x(y) = u_\infty f(y)$, $B_y(y) = B_\infty g(y)$. Then a stationary configuration is characterized by the inflow parameters u_∞, B_∞, or simply $u_\infty = M$ using the normalization $B_\infty = 1$, and the parameters u_0, B_0, Δ, δ describing the internal reconnecting current sheet, as illustrated in Fig. 8. While M is prescribed, the current sheet parameters depend on the internal dynamics and are functions of η, in particular. A homogeneous resistivity distribution is chosen to avoid additional complications arising from resistivity gradient effects. Reconnection is said to be independent of η, if for fixed boundary conditions the configuration, in particular the width Δ of the current sheet, does not depend on η (for sufficiently small η).

First consider the case of very weak driving, $M = E \lesssim \eta \ll 1$. We obtain an approximate stationary solution, $\partial_t \psi = M$, by expanding eqs. (5), (6) in M, which to lowest order gives

$$\mathbf{B} \cdot \nabla j = 0 \tag{37}$$

$$\mathbf{v} \cdot \nabla \psi = -M + \eta j \,. \tag{38}$$

If j vanishes asymptotically for $|\mathbf{x}| \gg 1$, eq. (37) implies $j = 0$ everywhere in an X-point configuration with open field lines. In this case there is a simple similarity solution

$$\psi = \frac{1}{2}\left(x^2 - y^2\right) \tag{39}$$

$$\phi = \frac{M}{2} \ln \left| \frac{x+y}{x-y} \right| . \tag{40}$$

The solution is, however, not valid on the separatrix $x = \pm y$, where $\omega = 4Mxy/\left(x^2 - y^2\right)^2$ becomes singular invalidating the approximation in eq. (37). Hence the current j cannot vanish on the separatrix, in particular not in the X-point, which also makes the resistive term ηj in eq. (38) finite. In this case the magnetic configuration in the vicinity of the neutral point is fundamentally changed as discussed in more detail in section 6.1. However, for $M \lesssim \eta$, i.e. $M/\eta = MS = Rm \lesssim 1$, using normalizations $B_0 = v_A = 1$, $L = 1$ in the definitions of S and Rm, the region affected is small, $\delta = O\left(\eta^{1/2}\right)$, such that the global configuration is still essentially described by eqs. (39), (40) (Biskamp, 1986).

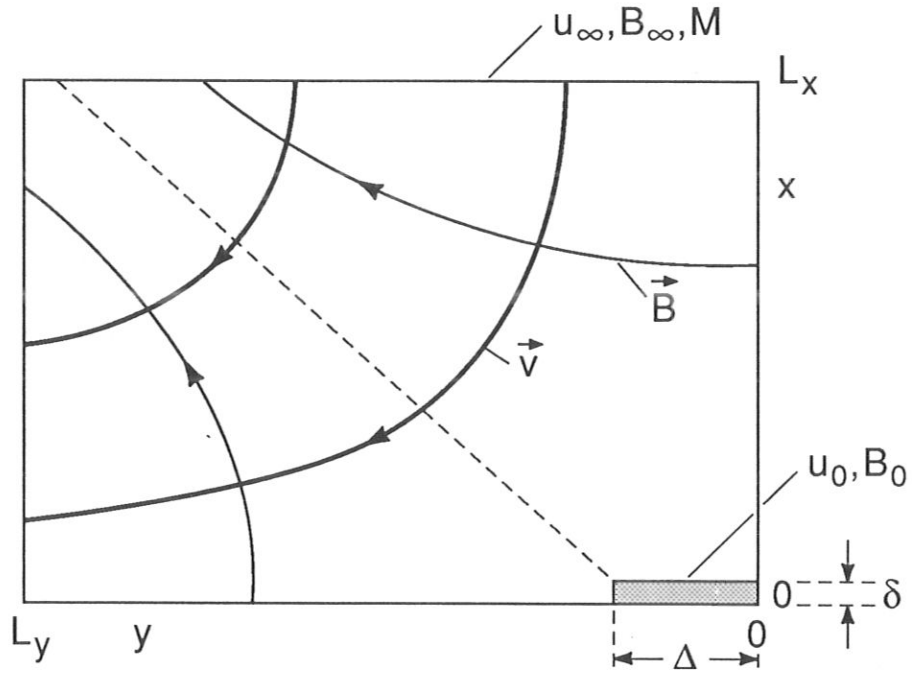

Figure 8: *Computational system and notation as used in numerical simulations of stationary driven reconnection.*

Increasing M at constant η or decreasing η at constant M, i.e. increasing $M/\eta \propto MS = Rm$, the magnetic Reynolds number*), to larger values, $Rm > O(1)$, the vicinity of the X-point is modified by the formation of a current sheet of certain width Δ.

A series of numerical simulations has been performed (Biskamp, 1986) for identical boundary profile functions, but different values of M and η. The

*)Note that the Reynolds number is defined by the fluid velocity $R_m = vL/\eta$, in contrast to the Lundquist number $S = v_A L/\eta$.

most conspicuous feature is the η-dependence of the width Δ of the internal current sheet. Figure 9 gives the flow pattern $\phi(x,y)$ and the magnetic configuration $\psi(x,y)$ for three cases differing only in the value of η. Obviously Δ increases rapidly with decreasing η until reaching the system size $\Delta \sim L$, in contrast to a Petschek-like behavior $\Delta = O(\eta)$. The current has the properties of a Sweet-Parker sheet, satisfying in particular relations (14) and (15). Quantitatively one finds the following M, η scaling laws for the variables B_0, u_0, Δ, δ of the internal current sheet

$$B_0 \propto M^2/\eta = MRm \tag{41}$$

$$u_0 = M/B_0 \propto Rm^{-1} \tag{42}$$

$$\Delta \propto M^4/\eta^2 = (MRm)^2 \tag{43}$$

$$\delta \propto M\eta^0 . \tag{44}$$

Hence increasing the Reynolds number Rm leads to an increase of the field B_0 in front of the sheet (flux pile-up) and a corresponding decrease of the upstream velocity u_0 because of the stationarity condition $uB = M$. The sheet width Δ *increases* with decreasing η and the thickness δ is independent of η contrary to expectation, and even *increases* with M because of the decrease of u_0, the deceleration of the upstream flow being apparent in Fig. 9c.

If the scaling laws (41) – (44) are universal and not just accidentally valid for the particular set of numerical simulations, they should reflect the physics of the Sweet-Parker current sheet, an important feature of which is the acceleration along the current sheet. Consider the average force along the sheet. Since v_y increases linearly $v_y \simeq B_0 y$, we have

$$\overline{v_y \partial_y v_y} \simeq B_0^2/2\Delta \simeq M/2\delta \tag{45}$$

using mass conservation $u_0\Delta = B_0\delta$ and Ohm's law $u_0 B_0 = M$. The scaling law (44) implies that the force along the sheet is invariant under changes of M and η, in particular remaining finite for $\eta \to 0$.

Finally we discuss the scaling of the energy dissipation rate W_η, compared with the input power W_{in}. Using eqs. (41) – (44) we obtain the following estimate

$$\begin{aligned} \frac{W_\eta}{W_{in}} &\simeq \int \eta j^2 dF \Big/ \int u B^2 dl \\ &\simeq \eta \frac{B_0^2}{\delta^2} \Delta\delta \Big/ u_\infty B_\infty^2 L_y \\ &\propto M^6/\eta^3 , \end{aligned} \tag{46}$$

since Ohmic dissipation is concentrated in the current sheet. W_η equals the magnetic field energy flux into the sheet $W_\eta \simeq u_0 B_0^2 \Delta$. Relation (46) indicates in particular that the fraction of the input power, which is dissipated, increases with decreasing η becoming of order unity for a macroscopic current sheet width.

When the current sheet width reaches the size of the global configuration $\Delta \simeq L$ as in Fig. 9c, the width Δ cannot increase further and the scaling laws (41) - (44) are no longer valid. In this case the scaling behavior is directly determined by the properties of the Sweet-Parker current sheet of width $\Delta = L$. From

$$u_0 B_0 = M \simeq \eta B_0 / \delta$$

one obtains

$$u_0 = \eta/\delta \quad , \quad B_0 = M\delta/\eta \, .$$

Inserting these results into the mass conservation equation $u_0 L = B_0 \delta$ yields the scaling relations

$$B_0 \propto \left(M^2 L/\eta\right)^{1/3} \tag{47}$$

$$\delta \propto \left(\eta^2 L/M\right)^{1/3} \tag{48}$$

$$A \propto \left(M L^2/\eta^2\right)^{1/3} \tag{49}$$

Examples of such current sheet reconnection processes are the coalescence of two magnetic islands and the nonlinear evolution of the resistive kink mode (section 8).

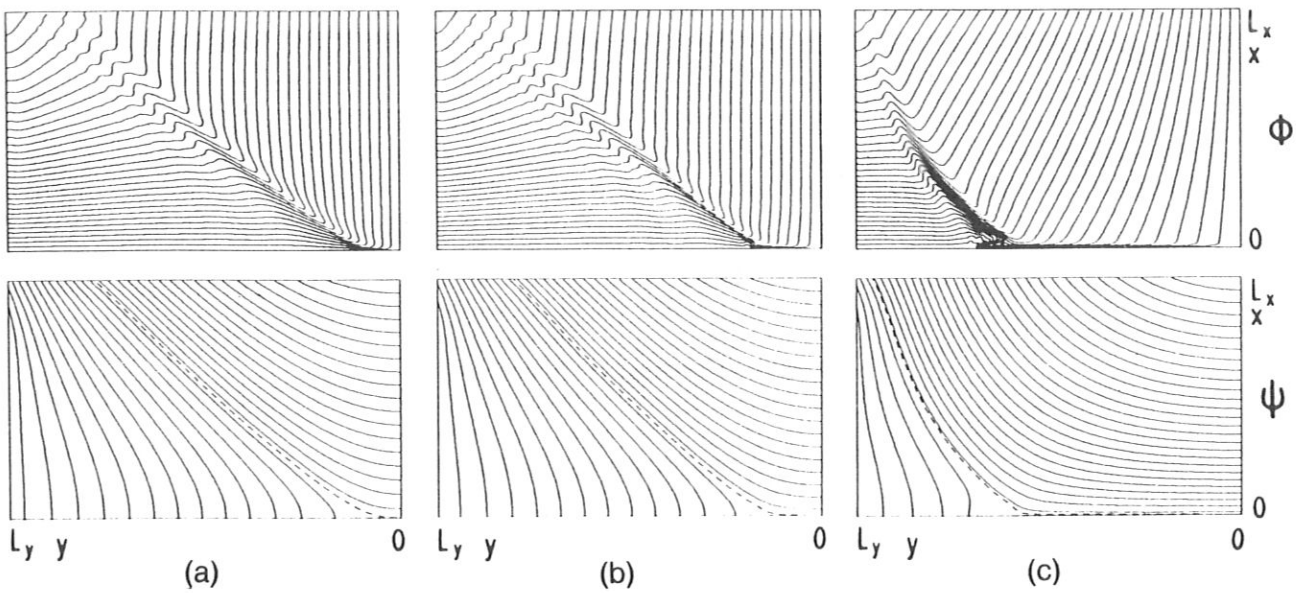

Figure 9: *Stream function $\phi(x,y)$ and flux function $\psi(x,y)$ for three stationary configurations of current sheet reconnection.*
(a) $\eta = \eta_0$; (b) $\eta = \eta_0/2$; (c) $\eta = \eta_0/4$ (from Biskamp, 1986).

6 Current sheets : refined theory

We have seen in the preceding section 5 that the diffusion region in stationary reconnection has the form of a current sheet, which may reach macroscopic size and which has the characteristic properties of a Sweet-Parker sheet. In this section we present a more detailed theory of the diffusion layer considering separately the central part and the edge region.

6.1 Stationary solution in the vicinity of the neutral point

The simplest way to investigate the solution of the resistive MHD equations in the vicinity of the neutral point $(x, y) = (0, 0)$ is to use a Taylor series expansion in x and y (Cowley, 1975; Shivamoggi, 1985). Assume a symmetric configuration indicated in Fig. 10a, where the stagnation point of the flow coincides with the neutral point of the magnetic field:

$$\begin{aligned} \psi &= \sum_{m,n} \psi_{2m,2n} \frac{x^{2m} y^{2n}}{(2m)!\,(2n)!} \\ \phi &= \sum_{m,n} \phi_{2m+1,2n+1} \frac{x^{2m+1} y^{2n+1}}{(2m+1)!\,(2n+1)!} \end{aligned}$$

$$f_{mn} = \partial_x^m \partial_y^n f|_{x,y=0} \;,\; f = \psi, \phi \,.$$

For stationary conditions eqs. (5), (6) read

$$\partial_x \phi\, \partial_y \psi - \partial_y \phi\, \partial_x \psi = \eta \left(\partial_x^2 \psi + \partial_y^2 \psi \right) - E \tag{50}$$

$$\partial_x \phi\, \partial_y \omega - \partial_y \phi\, \partial_x \omega - \partial_x \psi\, \partial_y j + \partial_y \psi\, \partial_x j = \mu \left(\partial_x^2 \omega + \partial_y^2 \omega \right) \,, \tag{51}$$

where $E \equiv \partial_t \psi = const.$ Since at the origin $\mathbf{B} = \mathbf{v} = 0$ and hence $\eta j = E$, eq. (50) gives

$$\eta \left(\psi_{20} + \psi_{02} \right) = E \,. \tag{52}$$

Differentiating eq. (50) twice with respect to both x and y at the orgin one obtains

$$2\phi_{11}\psi_{20} + \eta \left(\psi_{40} + \psi_{22} \right) = 0 \tag{53}$$

$$2\phi_{11}\psi_{02} - \eta \left(\psi_{22} + \psi_{04} \right) = 0 \,. \tag{54}$$

Differentiating eq. (51) once with respect to x and y at the origin gives

$$-\psi_{20}(\psi_{22}+\psi_{04})+\psi_{02}(\psi_{40}+\psi_{22})=\mu(\phi_{51}+2\phi_{33}+\phi_{15})\ , \tag{55}$$

which becomes by use of eqs. (53), (54)

$$-\frac{4}{\eta}\phi_{11}\psi_{20}\psi_{02}=\mu(\phi_{51}+2\phi_{33}+\phi_{15})\ . \tag{56}$$

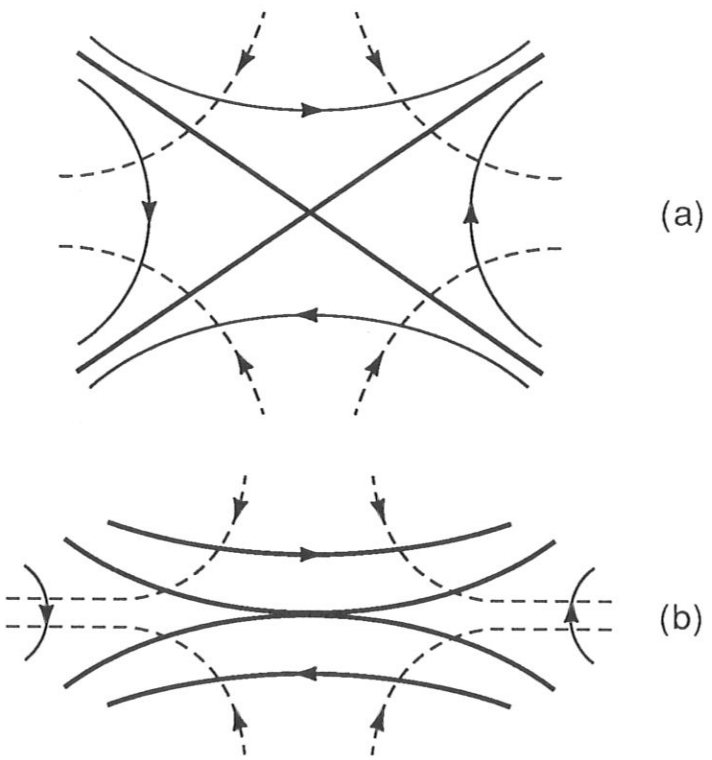

Figure 10: *Behavior of $\psi(x,y)$ (full lines) and $\phi(x,y)$ (dashed lines) in the vicinity of the neutral point. In the resistive case the separatrix branches cannot intersect at a finite angle (Fig. (a)), but osculate (Fig. (b)).*

First consider the inviscid case $\mu = 0$. Assuming $\phi_{11} \neq 0$, i.e. stream lines forming hyperbolae, either ψ_{20} or ψ_{02} (not both because of eq. (52)) must vanish. This implies that field lines are not hyperbolae, in particular the separatrices do not intersect at a finite angle, but osculate as indicated in Fig. 10b, where we chose $\psi_{20} \neq 0$, $\psi_{02} = 0$. While in an X-point configuration B_x in the downstream cones increases linearly, $B_x = \psi_{02} y$, it is cubic in the osculating configuration, $B_x \propto y^3$, whereas the velocity is in general linear, $v_y = \phi_{11} y$. This behavior indicates the inherent tendency to formation of current sheets in a resistive magnetized fluid.

In the case of finite viscosity these conclusions can no longer be drawn from eq. (56). In general ψ_{02} will be finite, its magnitude depending on the higher order terms in the Taylor expansion of the streamfunction, in particular ϕ_{51}, the dominating term in an elongated configuration with $\partial_x \gg \partial_y$. Numerical simulations, however, show that even for $\mu \sim \eta$ the inviscid behavior $B_x \propto y^3$ is still nearly valid, implying ϕ_{51} to be small, $\phi_{51} \ll \phi_{11}/\delta^4$, where δ is the sheet thickness, i.e. the current gradient scale defined by $\psi_{40} \sim \psi_{20}/\delta^2$.

Since the configuration around a neutral point tends to be stretched out, one can make use of the quasi-one-dimensional character $\partial_x \gg \partial_y$ by performing a power expansion only in y,

$$\psi(x,y) = \psi_0(x) + y^2 \psi_2(x)/2! + \cdots \tag{57}$$

$$\phi(x,y) = y\phi_1(x) + y^3 \phi_3(x)/3! + \cdots \ . \tag{58}$$

If the zeroth order current distribution $j_0(x) = \psi_0''(x)$ is given, the other functions $\psi_2(x), \ldots, \phi_1(x), \ldots$ can be determined successively in terms of $j_0(x)$. Let us assume the following profile

$$j_0(x) = \frac{j_m}{\cosh^2(x/\delta)} , \tag{59}$$

which is found in the simulations to fit the current density in the diffusion region surprisingly well, and calculate the first terms in the series (57), (58) explicitly. Integration of (59) gives

$$\psi_0(x) = j_m \delta^2 \ln[\cosh(x/\delta)] . \tag{60}$$

Inserted into eq. (50) one obtains

$$\phi_1(x) = (\eta/\delta) \tanh(x/\delta) \tag{61}$$

and hence the lowest order velocity components in the sheet

$$\begin{aligned} v_x^{(1)} &= -u_0 \tanh(x/\delta) \\ v_y^{(1)} &= u_0 (y/\delta) \cosh^{-2}(x/\delta) \, . \end{aligned}$$

Here $u_0 = \eta/\delta$ is the upstream velocity and $v_0 = B_0 = j_m \delta$ is the downstream velocity, which defines the width Δ of the sheet using the mass conservation relation $v_0 \delta = u_0 \Delta$. In fact the inverse aspect ratio of the sheet $\delta/\Delta = u_0/B_0 = \eta/(j_m \delta^2) \equiv M_0 \ll 1$ is the smallness parameter in the expansions (57), (58). The next order terms can be obtained by straightforward but somewhat tedious calculation using both equations (50), (51). For $\mu = 0$ one finds

$$\begin{aligned} \psi_2(x) &= -2M_0^2 j_m \left(\frac{1}{\cosh^2(x/\delta)} - 1 + \frac{x}{\delta} \tanh(x/\delta) \right) \\ \phi_3(x) &= M_0^3 \frac{j_m}{\delta} \left[\tanh(x/\delta) - \frac{3}{\cosh^2(x/\delta)} \left(\frac{x}{\delta} - 2 \tanh(x/\delta) \right) \right] \, . \end{aligned}$$

Since $\psi_2(x = 0) = 0$, we see that $B_x(x = 0, y)$ does not increase linearly in y but at most cubically. The same is true for the second order current density contribution $\psi_2''(x = 0) = 0$.

In order to obtain the variation of the current density along the y-axis one has to go to the fourth order, which yields

$$j(x = 0, y) = j_m \left[1 - \frac{4}{3} \left(M_0 \frac{y}{\delta} \right)^4 \right] \, . \tag{62}$$

This does, however, not contradict Syrovatskii's result eq. (36), where the line current density $J(y) = \int j(x, y) dy$ varies parabolically $J(y) \simeq 1 - ay^2$ for $y \ll b$. In fact eq. (62) is only valid along the center line of the sheet, the y-axis, where j_2 vanishes. The x-integrated second order contribution does not vanish. Instead one obtains

$$J(y) = 2 j_m \delta \left[1 - \left(\frac{M_0 y}{\delta} \right)^2 \right] \, . \tag{63}$$

Since $B_x \propto y^3$, the Lorentz force along the sheet is small, $B_x j \propto y^3$, such that the plasma acceleration is mainly due to the pressure force $-\partial_y p \simeq v_y \partial_y v_y \propto y$.

6.2 Current sheet edge region

Let us now discuss the behavior in the edge region of the current sheet $y \simeq \Delta$, where the Taylor series expansions (57), (58) break down, since $M_0 y/\delta$ becomes of order unity. Thus the only reliable information is obtained from direct numerical simulations. Earlier analytical treatments of the diffusion region (see e.g. Vasyliunas, 1975) assumed a smooth transition to the ideal exterior region of the downstream cone with the fluid continuing to flow at the upstream Alfvén velocity. However, such a highly super-Alfvénic flow (the local Alfvén velocity in the downstream cone is much smaller than in the upstream region) should be sensitive to shock formation, which would increase the field intensity and slow down the flow to sub-Alfvénic velocities. In fact simulations show, that the ideal downstream flow is clearly sub-Alfvénic and not related to the high speed reached *within* the diffusion region.

Closer inspection of the edge of the diffusion region reveals a complicated structure, as is illustrated in Figs. 11 and 12. Figure 11 gives stereographic plots of the current distribution viewed from the upstream side a) and the downstream side b), which reveal the main features of the configuration, the diffusion layer represented by the central current sheet along the y-axis, the weaker sheet current along the separatrix, reminiscent of a Petschek slow shock, both joining in a region of rather complex behavior, the edge region of the diffusion layer. As is seen in Fig. 11b the current density in the diffusion layer changes sign, i.e. the positive central part is followed by a negative part, terminated by a quasi-singular spike (numerically well resolved, however). Figure 12 gives contour plots of j, ϕ, ψ in the edge region of three stationary simulation states (the symmetric lower quadrant is added for clarity) with a) $\eta = \eta_0$, b) $\eta = \eta_0/\sqrt{2}$, c) $\eta = \eta_0/2$, showing the rapid increase of complexity as η is reduced. The point, where the current density of the diffusion layer changes sign (marked by the arrows in the j-plots) coincides with the location, where the separatrix (dashed line in the ψ-plots) branches off, as in Syrovatskii's current sheet configuration, Fig. 7a. The dynamics can most readily be interpreted when considering the ϕ-contours, high streamline density indicating high velocity. The flow, which is accelerated in the central current sheet up to the upstream Alfvén speed, is decelerated in the following part of reversed current density and finally completely blocked and turned backwards at the current sheet end point singularity, the spike in Fig. 11b. The flow is subsequently again accelerated forming two secondary current sheets parallel to the primary one, with the same characteristics, $j > 0$ part, $j < 0$ part and flow-blocking shock-like structure. In the limit $\eta \to 0$

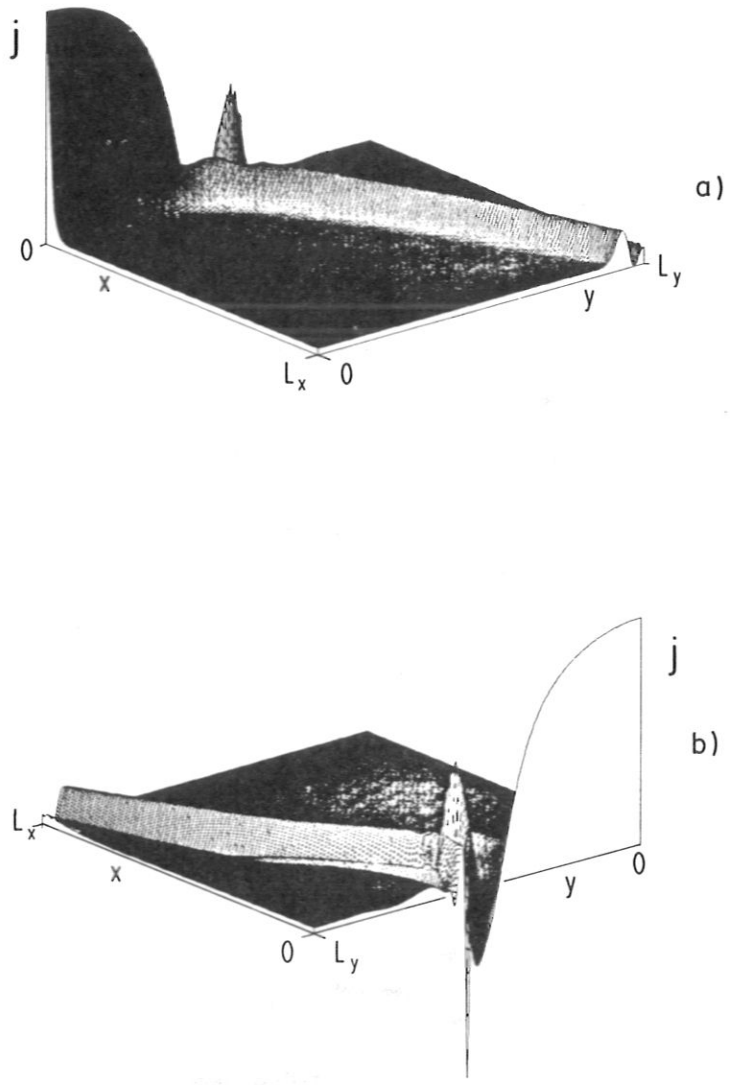

Figure 11: *Stereographic plots of the current distribution of a stationary reconnection configuration, (a) viewed from upstream side, (b) from the downstream side (from Biskamp, 1986).*

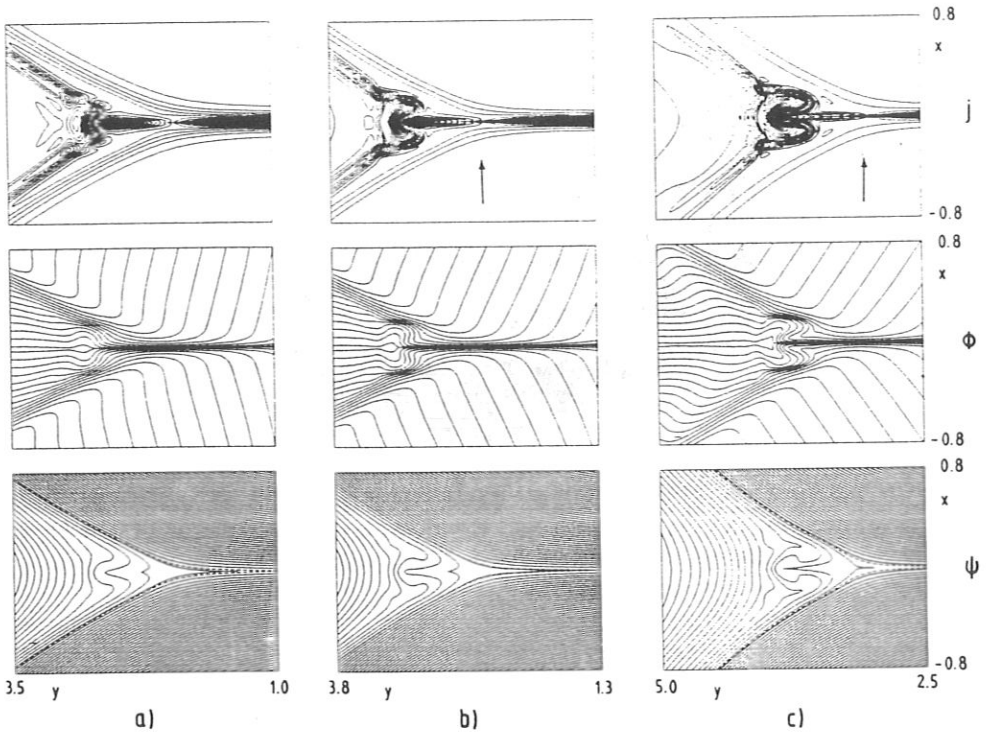

Figure 12: *Contours of j, ϕ, ψ in the edge region of the diffusion layer, (a) $\eta = \eta_0$; (b) $\eta = \eta_0/\sqrt{2}$; (c) $\eta = \eta_0/2$ (from Biskamp, 1986).*

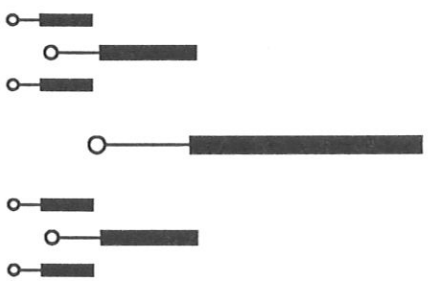

Figure 13: *Schematic drawing of the selfsimilar hierarchy of current sheets in the edge region of the diffusion layer:* ▬▬ *= positive j,* ——— *= negative j,* • *= endpoint singularity.*

a hierarchy of higher order current sheets seems to be generated with a selfsimilar scaling behavior as drawn schematically in Fig. 13.

The properties of the diffusion layer as revealed by numerical simulation and outlined in this section are consistent with Syrovatskii's current sheet model, the multi-current sheet edge behavior representing the dynamically resolved singularity predicted in Syrovatskii's quasi-static theory. The picture indicated in Fig. 13, however, rests on a twofold idealization. One is the assumption of perfect symmetry, the other that of stationarity. As will be discussed in section 8, a dynamic current sheet though much more stable than a static one becomes unstable, if the aspect ratio $A = \Delta/\delta$ is sufficiently large, giving rise to a nonstationary behavior. In a less symmetric configuration such nonstationary behavior would be very complex. In fact the most probable dynamic state is that of fully developed turbulence consisting of a statistical distribution of micro-current sheets (Biskamp and Welter, 1989). The stationary multiple current sheet configuration presented here gives a first indication about the complicated behavior to be expected at high Reynolds numbers.

7 Tearing instability of a Sweet-Parker current sheet

In a static sheet pinch, for which the tearing mode is usually considered (Furth et al., 1963), the instability condition $ka < 1$ implies that the configuration becomes unstable for aspect ratio $A = \Delta/a \gtrsim 2 \cdot 2\pi/ka \sim 10$. The existence of apparently stable current sheets of considerably larger A, as observed in numerical simulations, indicates that the dynamics involved in a Sweet-Parker sheet has a considerable stabilizing effect. The stability properties of such configuration with respect to the tearing mode were studied by Bulanov et al. (1979). Strictly speaking a Sweet-Parker sheet is a weakly two-dimensional system, where the inhomogeneity along the sheet arises because of the acceleration of the parallel flow as well as the increase of the normal magnetic field component. Since the latter is weak, $B_x \propto y^3$, as we have seen in section 6.1, the inhomogeneity of the parallel flow is the dominant effect,

$$v_y(y) = \Gamma y\,, \tag{64}$$

where

$$\Gamma = v_A/\Delta \simeq u/\delta \simeq \eta/\delta^2\,,$$

using the properties of a Sweet-Parker sheet. Hence Γ^{-1} is just the resistive time τ_R of the current sheet and the aspect ratio equals the Lundquist number of the sheet,

$$\Delta/\delta = v_A \delta/\eta = \tau_R/\tau_A \equiv S_\delta \,, \tag{65}$$

where the subscript δ should remind the reader that S_δ is to be distinguished from the Lundquist number $S = v_A L/\eta$ of the global configuration, $S_\delta \ll S$ usually. The normal component of the flow u only has the effect of balancing resistive broadening of the sheet. Being zero at the sheet centerline $x = 0$, the resonant surface of the tearing mode, it does not affect tearing mode stability, nor does the shear of the parallel flow $v_y(x)$, since it, too, vanishes on the centerline $\partial_x v_y|_{x=0} = 0$.

Bulanov et al. apply a WKB analysis which results in a relatively complicated formalism, the strict evaluation of which does not appear to be very rewarding. Syrovatskii (1981) has summarized the results giving a simple stability condition

$$\Gamma \gtrsim \gamma \,, \tag{66}$$

where γ is the tearing mode growth rate for a one-dimensional static sheet. The result (66) can easily be understood. The tearing mode corresponds to a local current condensation, which is counteracted by the wavelength stretching caused by the inhomogeneous parallel flow. More quantitatively, one may assume that the mode is effectively stabilized, if the relative change of the wavelength during one e-folding time exceeds, say, $1/4$:

$$\left(v_y\left(y+\lambda\right) - v_y\left(y\right)\right)/\gamma\lambda = \Gamma/\gamma > 1/4 \,. \tag{67}$$

Hence the sheet is tearing mode stable, if $\Gamma > \gamma_{max}/4$. In the asymptotic limit of large S one has $\gamma_{max} \simeq 0.6\left(\tau_A \tau_R\right)^{-1/2}$ (Furth et al., 1963), valid for $k_m \delta \simeq S_\delta^{-1/4}$, which by use of eq. (65) gives the stability condition

$$\tau_R^{-1} \gtrsim 0.15\left(\tau_R \tau_A\right)^{-1/2}$$

or

$$\delta/\Delta \gtrsim 2 \times 10^{-2} \,. \tag{68}$$

Since for relatively low S-values, $S_\delta \equiv \Delta/\delta < 10^2$, γ_{max} is somewhat smaller than predicted by the asymptotic formula, and because of the semi-quantitative nature of the criterion (67) we may say, that the tearing mode is unstable for current sheet aspect ratio $\Delta/\delta \gtrsim 10^2$.

In addition stability is expected to depend on the magnitude of the perturbation. Since the equilibrium flow, which constitutes the stabilizing effect, is affected by a finite perturbation amplitude, the current sheet may actually tear for smaller aspect ratios than predicted by linear theory. In numerical simulations a current sheet configuration appears to be more prone to tearing when a poorer spatial resolution is used, since discreteness effects generate a higher noise level. Finally also the lack of stationarity, which is to be expected for general reconnection systems, leads to a higher sensitivity with respect to the tearing mode.

From the scaling laws for driven reconnection eqs. (43), (44) $\Delta/\delta \sim \eta^{-2}$, or (49), $\Delta/\delta \sim \eta^{-2/3}$, we see that the tearing mode will be unstable in a Sweet-Parker sheet for sufficiently small η. Let us therefore consider its nonlinear behavior. Though there are cases, where a chain of several magnetic islands of comparable size is generated similar to the tearing mode in a one-dimensional static sheet pinch, more typically only one isolated island is generated in the most unstable center part of a dynamic current sheet. While growing in width and thickness in a rather selfsimilar way it is convected along the sheet and expelled into the downstream region. Such isolated island is now generally called a plasmoid. Figure 14 illustrates the repetitive generation and evolution of plasmoids. Shown is a configuration of driven reconnection as given in Fig. 10 (for clarity the lower symmetric part is added in the plot). Changing the boundary conditions at $y = 0$ slighty from $\partial_y \psi = 0$ to $\psi(x,t) = \psi(x) + Mt$, where M is the externally imposed average reconnection rate and $\psi(x)$ is the stationary ψ distribution on the axis $y = 0$ observed in the case c) of Fig. 10, is sufficient to generate a periodic sequence of plasmoids. The properties of plasmoids and their acceleration, which plays an important role in the earth's magnetotail, will be considered more closely in section 8.3.

8 Examples of 2-D reconnecting system

In this section we consider in more detail some typical dynamic systems, which develop fast reconnection, either as a result of an instability of the initial configuration in the cases of the coalescence instability and the resistive kink instability, or by a lack of equilibrium of the configuration in the case of plasmoid acceleration.

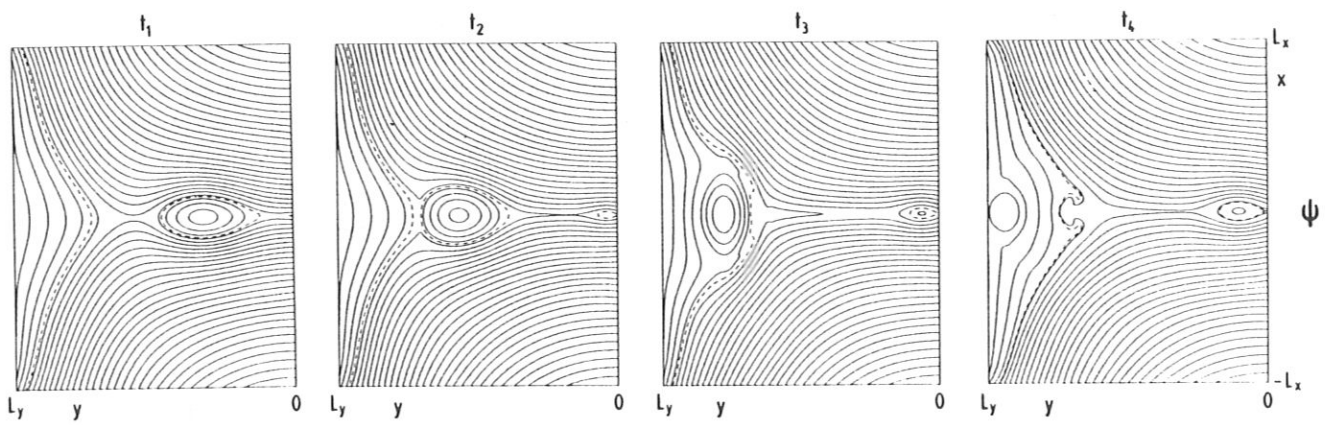

Figure 14: *Repetitive plasmoid generation in a tearing unstable Sweet-Parker current sheet. The figure shows ψ-contours at times $t_1 < t_2 < t_3 < t_4$ (from Biskamp, 1986).*

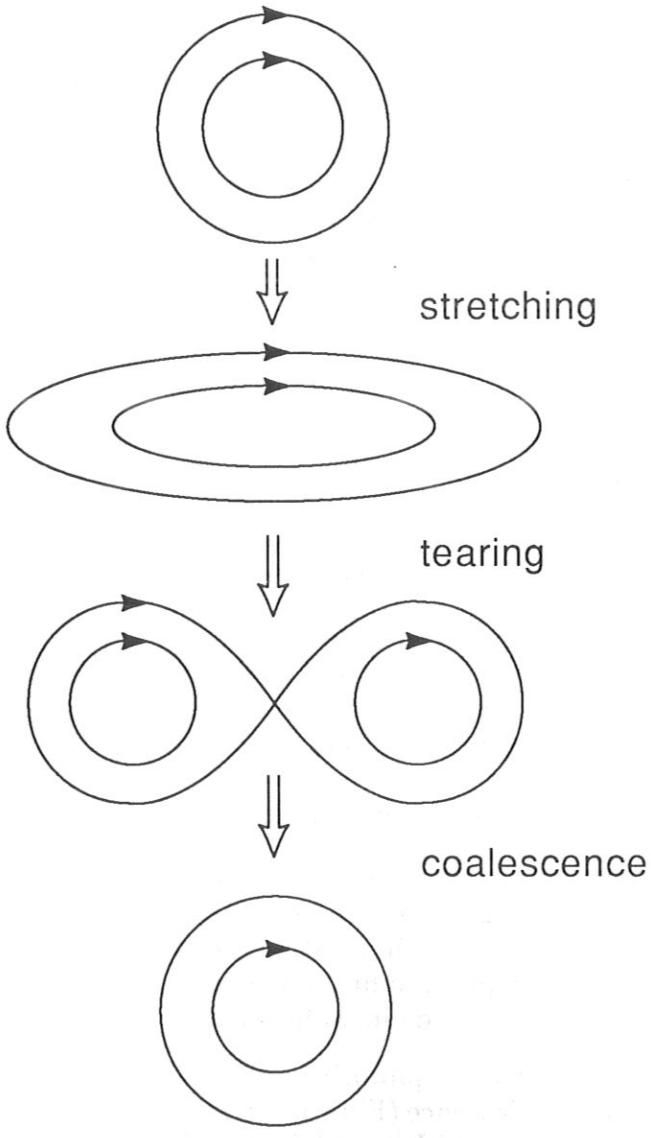

Figure 15: *A circular pinch forced into an elongated shape tends to restore its original shape by tearing and subsequent coalescence (schematic drawing).*

8.1 Coalescence of magnetic islands

There are essentially two types of dynamic processes, which may occur in an evolving two-dimensional magnetic configuration, tearing and coalescence. The natural plasma shape is that of circular cross section, the cylindrical pinch. If such a system is forced into an elongated shape, it will tear, i.e. break up into two or more fractions of about circular cross section, which will subsequently coalesce to restore the original configuration as illustrated in Fig. 15. Both processes are basically driven by the same physical effect, the attractive force between parallel currents. Tearing is usually a slow process. It corresponds to a local condensation or nucleation of the current density in a conducting medium, which from the beginning has to overcome the ideal flux conservation constraint by reconnection and hence cannot build up momentum to drive reconnection at a rate substantially faster than that of global resistive diffusion. By contrast, coalescence is a fast process. The currents flowing in the two flux tubes exert a finite attractive force on each other, which drives reconnection at a faster rate.

The coalescence process has been studied starting from a periodically corrugated sheet pinch equilibrium consisting of a sequence of magnetic islands as shown in Fig. 3.7 (Pritchett and Wu, 1979; Biskamp and Welter, 1980). It belongs to the class of equilibria (Fadeev et al., 1965),

$$\psi(x,y) = B_\infty a \ln\left(\cosh\left(x/a\right) + \varepsilon\cos\left(y/a\right)\right) , \tag{69}$$

where B_∞ is the asymptotic field for $|x| \to \infty$, and ε is a measure of the equilibrium island size w_0, given by the equation $\cosh\left(w_0/2a\right) = 1 + 2\varepsilon$, $w_0/a \simeq 4\sqrt{\varepsilon}$ for $w_0 \ll a$. It is interesting to note that the equilibrium eq. (69) corresponds to a finite amplitude tearing mode with wave number $ka = 1$, the marginally stable mode in an uncorrugated ($\varepsilon = 0$) sheet pinch.

It has been shown that the equilibrium (69) is ideally unstable with respect to pairwise island coalescence (Finn and Kaw, 1977) for any equilibrium island size $w_0 > 0$ (Pritchett and Wu, 1979). The nonlinear dynamic process has been investigated numerically, by solving the incompressible 2-D MHD equations (5), (6). It can be divided into an ideal MHD phase, where the plasma within the islands are freely accelerated toward each other leading to field compression and the formation of a sheet current between the islands, and a quasi-stationary reconnection phase. For intermediate values of the normalized resistivity $\eta = S^{-1}$, typically $10^{-2} - 10^{-4}$, a selfsimilar behavior is observed, with the following η-scaling laws for the upstream quantities u_0,

B_0 taken just in front of the diffusion layer:

$$\begin{aligned} u_0 &\propto \eta^{1/3} \\ B_0 &\propto \eta^{-1/3} \end{aligned} \tag{70}$$

and the width Δ and thickness δ of the layer

$$\begin{aligned} \Delta &\simeq w_0 \propto \eta^0 \\ \delta &\propto \eta^{2/3}. \end{aligned} \tag{71}$$

As a consequence the reconnection rate computed at the X-point, $\dot{\psi}_X = \eta j_X = u_0 B_0$, is independent of η. This does, however, not mean, that the reconnection process can be associated with a Petschek-like behavior. In fact there is no relationship, since reconnection occurs in a macroscopic current sheet, $\Delta \simeq w_0$. Relations (70), (71) agree with the scaling laws for driven reconnection (47) – (48), since the equivalent driving M produced by the coalescence instability is large enough for $\eta < 10^{-2}$ to generate a current sheet of the global system size, i.e. the equilibrium island width w_0. A typical state is illustrated in Figs. 16 and 17.

Obviously the eqs. (70) are only valid for a certain η-range, since the value of the field B_0 cannot exceed the maximum value B_m, which would be obtained in the ideal case $\eta = 0$ for $u_0 = 0$, when the inward motion is reversed because of the repelling force produced by the compressed field. Hence the scaling law eq. (70) breaks down, if B_0 approaches B_m. For smaller values of η, typically $\eta < 10^{-4}$, one finds a Sweet-Parker scaling law

$$\overline{u}_0 \propto \eta^{1/2}$$

$$\overline{B}_0 \simeq B_m \propto \eta^0,$$

$\overline{u}_0$, $\overline{B}_0$ indicating a time average, since in this regime the motion of the island plasma toward the diffusion layer is increasingly modulated by an internal oscillation or sloshing owing to the finite kinetic energy obtained in the first phase of the instability. The behavior is illustrated in Fig. 18, showing the change $\Delta x(t)$ of the position of the O-point during coalescence, $\Delta x = 0$ corresponding to the initial two-island equilibrium state, $\Delta x = -\pi$ to the final one-island state for three values of the resistivity. While in the first phase $t \lesssim 90$, the ideal process of island acceleration, Δx is independent of η, in the subsequent phase dominated by current sheet reconnection one finds in fact $d\Delta x/dt \simeq const. \propto \eta^{1/2}$.

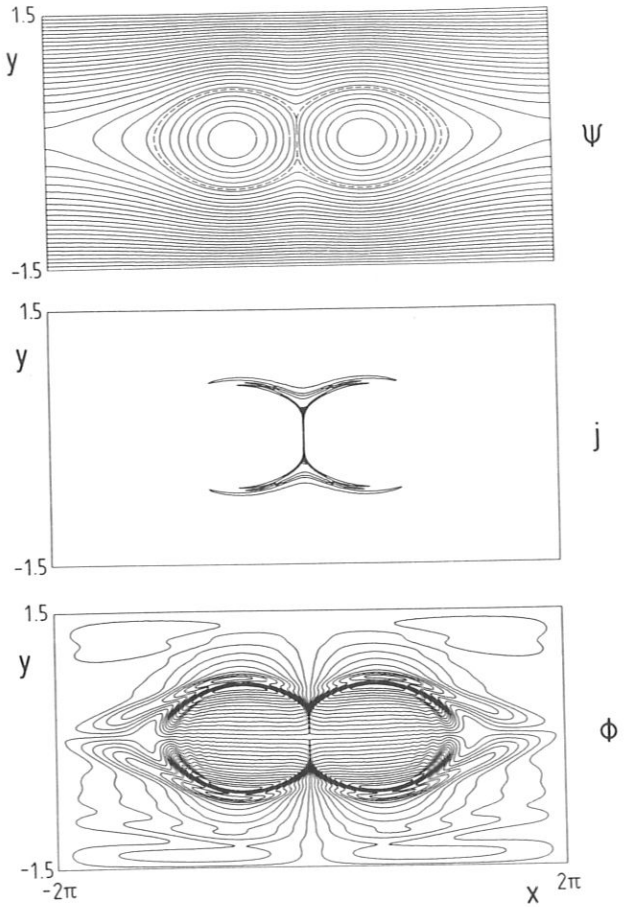

Figure 16: *Contours of ψ, j, ϕ during island coalescence.*

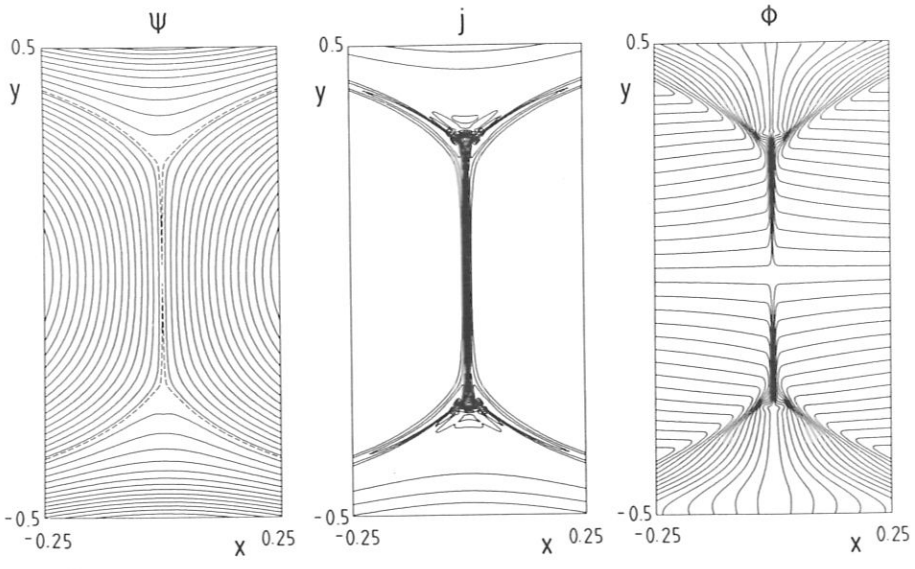

Figure 17: *Blow-up of the center region of the configuration shown in Fig. 16.*

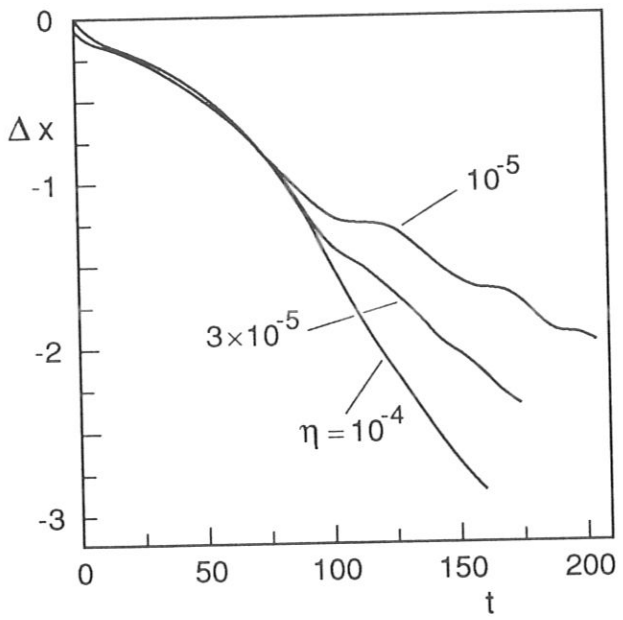

Figure 18: *Change of O-point position $\Delta x(t)$ during island coalescence for $\eta = 10^{-4}$, 3×10^{-5}, 10^{-5}.*

8.2 Nonlinear evolution of the resistive kink mode

It is well known that the linear theory of the $m = 1$ resistive kink mode in a cylindrical plasma column differs significantly from the $m \geq 2$ tearing mode (e.g. Ara et al., 1978). The physical reason is, that the latter corresponds to an ideally strongly stable mode, while the ideal $m = 1$ mode is usually close to marginal stability or even unstable. Hence it is driven by the free energy of the ideal mode and a more rapid nonlinear evolution than the diffusive growth of the tearing mode can be expected.

First consider the properties of the magnetic island produced by a finite amplitude $m = 1$ eigenmode. For simplicity we restrict ourselves to the case

of marginal ideal stability $\gamma_H = 0$. Let us first modify eqs. (5), (6) to describe the helical structure of the kink mode. Instead of the poloidal flux ψ one introduces the helical flux function ψ_*, which in the limit of a strong axial field B_0 reads (Kadomtsev and Pogutse, 1974)

$$\psi_* = \psi - \alpha B_0 r^2/2 \tag{72}$$

where α is the helical parameter, all quantities depending only on r and $\theta' = \theta - \alpha z$. In a large aspect ratio tokamak with major radius R we have $\alpha = R^{-1}$. The equations replacing eqs. (5), (6) read

$$\partial_t \psi_* + \mathbf{v} \cdot \nabla \psi_* = \eta j - \eta_2 \nabla^2 j \tag{73}$$

$$\partial_t \omega + \mathbf{v} \cdot \nabla \omega = (\mathbf{e}_z \times \nabla \psi_*) \cdot \nabla \nabla^2 \psi_* + \mu \nabla^2 \omega \; . \tag{74}$$

Note that these equations, in contrast to eqs. (5), (6) are not the general incompressible MHD equations in helical geometry, but require in addition the condition $B_0 \gg B_z$. Equations (73), (74) can easily be derived from the 3-D reduced equations (7), (8).

In the vicinity of the rational surface $r = r_1$, $x = r - r_1 \ll r_1$, the helical flux function ψ_* following the equation

$$(\partial_t + \mathbf{v} \cdot \nabla)\, \psi_* = \eta \left(\nabla^2 \psi_* + 2\alpha B_0 \right) \; ,$$

has the form

$$\psi_* \simeq \frac{1}{2} \psi_0'' x^2 + \psi_1(x) \cos\theta \; . \tag{75}$$

If the displacement ξ is larger than the resistive layer width δ_l, the island size exceeds δ_l. (The subscript l is introduced to distinguish the linear layer width $\delta_l \propto \eta^{1/3}$ from the sheet thickness in the nonlinear regime $\delta \propto \eta^{1/2}$.) Assuming that the form of the magnetic perturbation $\psi_1(x)$ is not broadened nonlinearly as in the case of the tearing mode, which will be seen below, the shape of the island can be calculated using the asymptotic form ($\delta_l \to 0$) of the eigenfunction $\psi_1(x)$:

$$\psi_1(x) = \begin{cases} \psi_0'' \xi x & x < 0 \\ 0 & x > 0 \, , \end{cases} \tag{76}$$

where ξ is the uniform displacement of the plasma inside the $q = 1$ surface. The magnetic configuration is illustrated in Fig. 19. The condition $\nabla \psi_* = 0$ gives the O-point of the island at $x = -\xi$, $\theta = 0$. The two branches of the

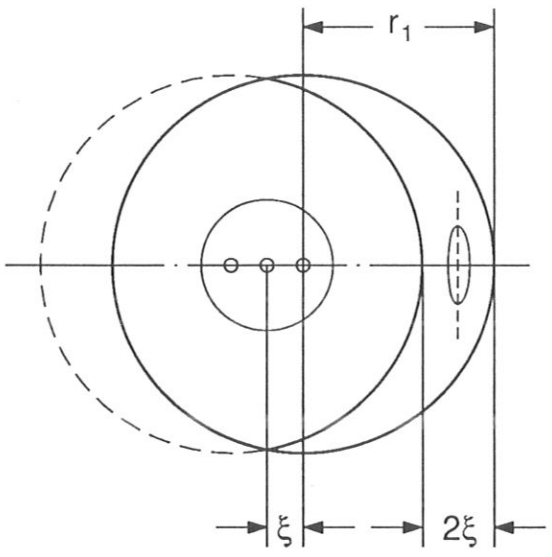

Figure 19: *Schematic drawing of the island shape caused by a central displacement ξ in the nonlinear resistive kink mode.*

separatrix are obtained by considering the flux surfaces passing through the "X-point" at $x = 0$, $\theta = \pi$. They have the value $\psi_* = 0$, i.e.

$$\begin{aligned} \frac{x^2}{2} + \xi x \cos\theta = 0 \qquad & x < 0 \\ \frac{x^2}{2} = 0 \qquad & x > 0\,. \end{aligned}$$

Hence the outer separatrix is given by the concentric circle

$$x = 0\,,$$

while the inner separatrix is given by

$$\begin{aligned} x = -2\xi\cos\theta \qquad & |\theta| < \pi/2 \\ x = 0 \qquad & |\theta| > \pi/2\,, \end{aligned}$$

i.e. consists of a shifted half-circle of the same radius as the outer separatrix for $|\theta| < \pi/2$ and coincides with the latter for $|\theta| > \pi/2$. This part represents a current sheet, the δ-function singularity in $\psi_1''(x)$ implied in eq. (76). While

the current sheet is sustained for $|\theta| > \pi/2$ owing to the impinging plasma flow, it is smeared out over the island for $|\theta| < \pi/2$, since here the plasma flow is receding. Hence eq. (76) is strictly speaking only valid for $|\theta| > \pi/2$, while for $|\theta| < \pi/2$ the perturbation is smoothed across the island, the size of which is

$$w = 2\,\xi\ . \tag{77}$$

The current sheet, the magnetic configuration, and the flow pattern obtained from an exact simulation are given in Fig. 20. Hence the nonlinear reconnection process occurs in a quasi-stationary current sheet of half-width $\Delta \simeq \pi r_1/2$.

In order to compute the nonlinear evolution $w(t)$, we adjust the simple plane Sweet-Parker reconnection model outlined in section 3.1 to the geometry of the kink mode. In the laboratory frame the flow into the current sheet is not symmetric, but enters only from the interior region, as seen in Fig. 20c. Since the reconnection of the helical field is necessarily symmetric involving equal positive and negative amounts of field, the current sheet itself is moving outward with the velocity $u/2$, where $u = \dot{\xi}$ is the plasma velocity in the laboratory frame, such that in the frame of the sheet the inflow velocity is $u_0 = u/2$. The continuity equation yields the relation

$$\int_0^{\pi/2} u_{0n} r_1 d\theta' = u_0 r_1 = v_0 \delta\ , \tag{78}$$

where $v_\theta = v_0$ is the outflow speed and δ the sheet half-thickness and we have inserted the normal component $u_{0n} = u_0 \cos\theta'\ , \theta' = \pi - \theta$.

The outflow speed v_0 equals the upstream Alfvén velocity computed with the field component to be reconnected (see eq. (13))

$$v_0 = B_*\ , \tag{79}$$

where B_* is the helical field in front of the sheet. B_* can most easily be obtained from the behavior of the helical flux $\psi_*(r, \theta = \pi)$ shifted rigidly toward the sheet as illustrated in Fig. 21,

$$B_* = |\partial_r \psi_*| = |\psi_0''|\,\xi/2 = |\psi_0''|\,w/4\ . \tag{80}$$

The total change of the helical field across the sheet $[B_*] = 2B_*$ agrees with the expression obtained from eqs. (75) and (76).

In contrast to a plane current sheet the inflow velocity u_{0n} is not homogeneous and hence the thickness δ is not constant but varies along the sheet,

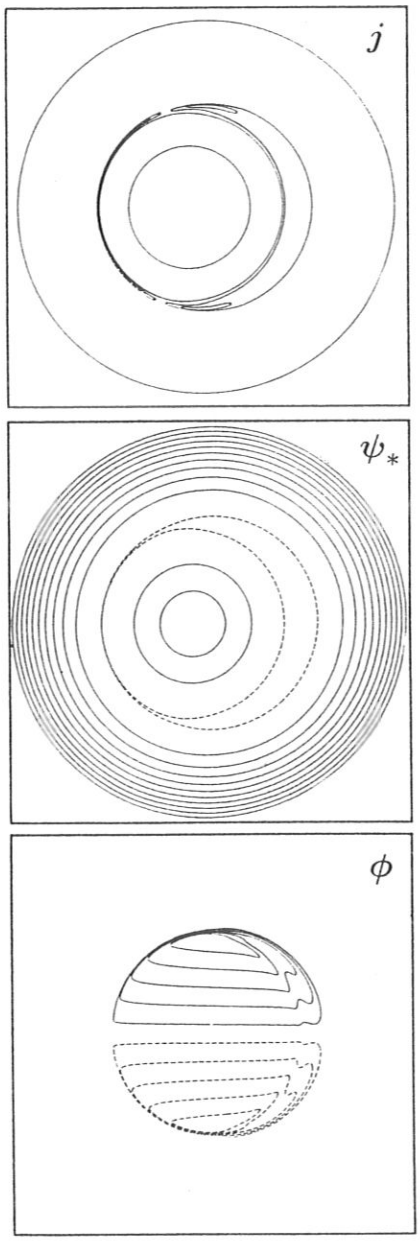

Figure 20: *Contour plots of (a) current density, (b) helical flux ψ_*, (c) stream function ϕ, for a simulation of the nonlinear resistive kink mode with $S = 10^7$ (from Biskamp, 1991).*

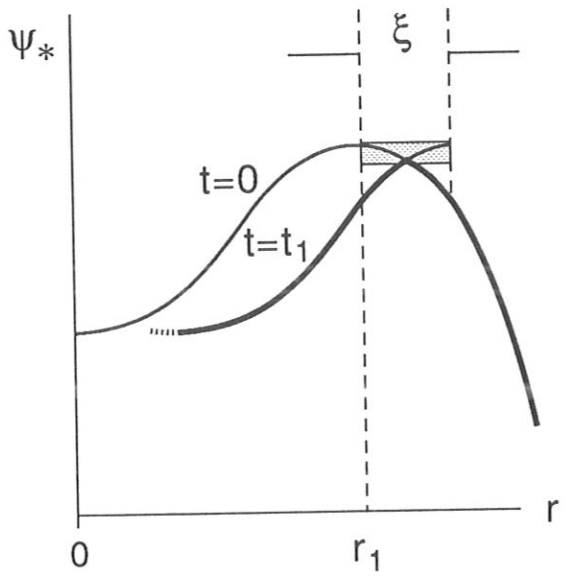

Figure 21: *Helical flux $\psi_*(r, \theta = \pi)$ (heavy line) resulting from a rigid shift of the interior branch which leads to a jump in the helical field B_*. The reconnected flux is indicated by the shaded area.*

$\delta = \delta(\theta)$. This is determined by Ohm's law for stationary conditions across the sheet, generalizing eq. (10),

$$u_{0n}(\theta)\ B_*(\theta) = \eta\ j(\theta) \simeq \eta\ \frac{B_*(\theta)}{\delta(\theta)} \tag{81}$$

and hence

$$\delta(\theta) = \eta / u_0 \cos\theta' \ . \tag{82}$$

Evidently the current sheet cannot extend up to $\theta' = \pi/2$, but only to some value $\theta_0 < \pi/2$. Simulations give a value $\theta_0 \simeq 0.8\pi/2$, as seen in Fig. 20a. Because of the broadening of the sheet the behavior in the edge region is rather smooth compared with the quasi-singular structure encountered in a plane current sheet (Figs. 11, 12), the negative current density part being only weakly pronounced in Fig. 20a.

Inserting eqs. (79), (80) and (82) with $\theta' = \theta_0$ into eq. (78) and using $u_0 = u/2 = \dot{w}/4$, one obtains the equation for the time evolution of the island

$$\dot{w} = 2\left(\eta\,|\psi_0''|\,w/r_1\cos\theta_0\right)^{1/2} \tag{83}$$

which yields the algebraic growth law for small but finite island size (Waelbroeck, 1989; Biskamp, 1991)

$$w = \eta\,|\psi_0''/r_1\cos\theta_0|\,t^2 \tag{84}$$

or

$$u = \eta\,|\psi_0''/r_1\cos\theta_0|\,t\ . \tag{85}$$

The nonlinear time scale obtained by setting $w \simeq r_1$ is $\tau = O(\eta^{1/2})$. Though the flow velocity into the sheet is small, $u \lesssim O(\eta^{1/2})$ as seen from eq. (85), inertia is not negligible, since the velocity along the sheet v_0 is independent of η.

Equation (85) is in quantitative agreement with results obtained from numerical simulations, performed with an initial j-profile

$$j = \left(1 + \left(\frac{r}{r_0}\right)^2\right)^{-2}$$

with $r_0 = 0.7$, $q = 1$ surface at $r_1 = 0.5$, and $\eta(r) = \eta_0/j(r)$. Figure 22 shows the velocity of the plasma center $u(t)$ (center curve) for $\eta_0 = 10^{-7}$. For reference the upper (dashed) curve represents continued exponential growth, while the lower curve represents the quasi-linear approximation, where u saturates, $u_{ql} \sim \gamma\delta_l = O(\eta^{2/3})$, in contrast to the exact behavior, where $u(t)$ grows linearly reaching $u_{max} = O(\eta^{1/2})$. From Fig. 22 one finds $u/a = t - t_0$ with $a \simeq 4 \times 10^{-7}$, while eq. (85) with $\theta_0 = 0.8\pi/2$ yields $a = 3.3 \times 10^{-7}$. Since the exact value depends on details such as the profiles of the sheet current and the flow, a simple exact theory as Rutherford's for the tearing mode cannot be obtained. It should be mentioned that naive application of Sweet-Parker reconnection theory without taking into account the geometric particularities of the kink mode gives the same scaling as eq. (84) but the numerical coefficient is smaller by roughly a factor of 10.

The resistive kink mode does not saturate at a finite island size but island growth proceeds until the entire helical flux originally inside the resonant surface $r = r_1$ is reconnected and the system effectively returned to a symmetric state. This is the basic model of the sawtooth relaxation oscillation in tokamaks.

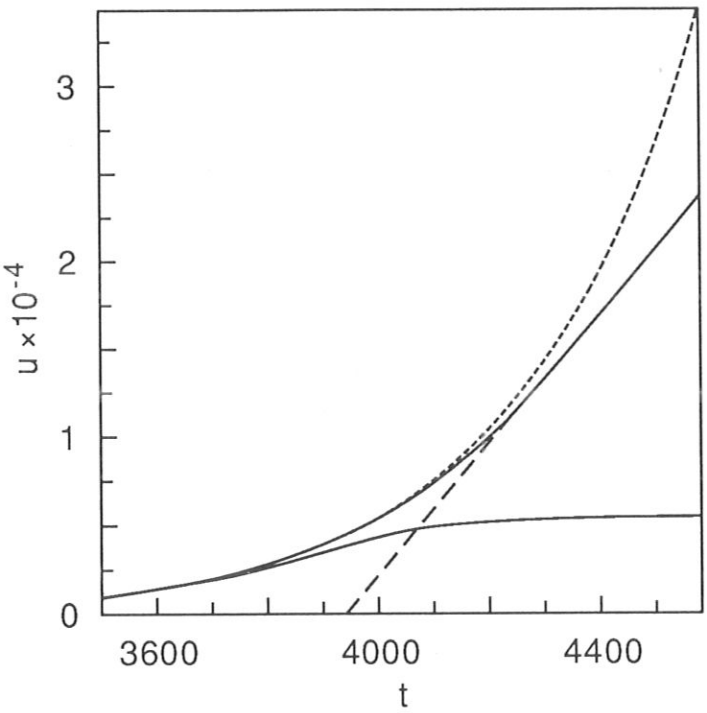

Figure 22: *Time evolution of the velocity u in the resistive kink mode (from Biskamp, 1991).*

8.3 Plasmoids

As indicated in section 7 the nonlinear evolution of the tearing mode in an open, weakly two-dimensional current sheet differs significantly from that in periodic systems. In the latter there is a chain of islands, for instance a $(m, n) = (m_0, 1)$ mode in a cylindrical configuration (no island coelescence is possible because of $n = 1$ corresponding to the largest possible wavelength), which grow slowly on the global resistive time scale (Rutherford, 1973). Since inertia effects are negligible, the process constitutes a sequence of smooth equilibrium states. By contrast in an open sheet configuration usually a single major plasmoid is generated, which is rapidly moving along the sheet while growing in size; an example was given in Fig. 14. Inertia effects are

important, since the system is not in MHD equilibrium, which allows much faster reconnection . Let us consider this process in more detail.

Plasmoids seem to be an important feature of various kinds of eruptive processes in astrophysical plasmas, notably magnetospheric substorms and solar flares. In fact in the dynamic numerical modelling of the earth's magnetotail plasmoid formation, which is believed to be the origin of the substorm phenomemon, has been investigated most intensely (Birn and Hones, 1981; Lee et al., 1985; Hautz and Scholer, 1987; Ugai, 1989; Otto et al., 1990; Kageyama et al., 1990).

The basic process is illustrated in Fig. 23. A weakly two-dimensional static equilibrium is assumed as initial state, modelling a typical magnetotail configuration. Equilibrium pressure variations along the tail midplane are usually chosen in such a way, that the configuration has a distant (from the earth, the left-hand boundary at $y = 0$) X-point. This X-point is useful in order to unambiguously define the volume, mass and momentum of the plasmoid (Otto et al., 1990), but seems to have little effect on the global plasmoid dynamics.

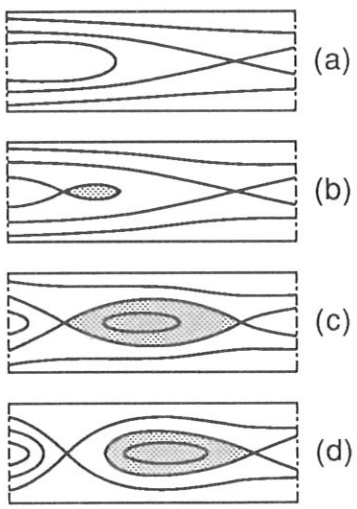

Figure 23: *Schematic drawing of the plasmoid evolution in a weakly two-dimensional magnetic configuration.*

Figure 24 gives a sequence of plasmoid states from a two-dimensional compressible MHD simulation by Hautz and Scholer (1987). (Because of finite plasma compressibility the flow pattern cannot be visualized by contour plots of a streamfunction ϕ, but requires a vector representation.) For finite resistivity the initial configuration is unstable to tearing. By applying a field perturbation or by locally increasing η one initiates reconnection at a particular position y_0 ($y_0 = 25$ in Fig. 24a), creating an X-point, thus starting the plasmoid formation. The plasmoid is accelerated along the sheet in the direction of decreasing pressure and field intensity. Since this motion leads plasma away from the X-point, it has to be replenished by motions from above and below into the X-point region, giving rise to a quasi-forced reconnection process, which continues on the fast Sweet-Parker time scale instead of slowing down to the global resistive time scale as in the case of a periodic tearing mode. In fact a long current sheet is created extending up to the receding plasmoid (Fig. 24b). Though the original distant X-point is hardly visible any more, the plasmoid volume is rather well defined by the flow pattern, the velocity being large and nearly uniform over the plasmoid cross-section. Interaction with the downstream plasma still at rest leads to shock formation (not well visible in Fig. 24) and a blunt leading plasmoid edge, which gives the plasmoid a drop-like shape and decreases the plasmoid acceleration. When the trailing current sheet is long enough, it becomes tearing unstable itself, producing secondary plasmoids, which are strongly accelerated toward the primary one and eventually coalesces with the latter (Figs. c,d). Three-dimensional effects do not change the general picture qualitatively as shown for instance by Kageyama et al. (1990), who present a global simulation of the interaction of the solar wind magnetic field with the magnetosphere. A long tail is formed giving rise to the continuous generation of plasmoids.

The question, concerning the dominant force in the plasmoid acceleration has been investigated by Otto et al. (1990). It turns out that the pressure force is significantly larger than the magnetic tension, which is similar to the plasma acceleration along a simple Sweet-Parker current sheet (section 6.1).

While the plasmoid acceleration is essentially an ideal MHD process, the reconnection time scale τ and hence the plasmoid growth depend on the value of η, roughly $\tau \sim S^{1/2}$. This implies that plasmoid size decreases with η. In most magnetotail simulation studies this fact is concealed by the use of an anomalous resistivity model with $\eta \propto j$. It should also be mentioned, that the basic problem in the theory of magnetospheric substorms is indeed the identification of the relevant dissipation process in Ohm's law.

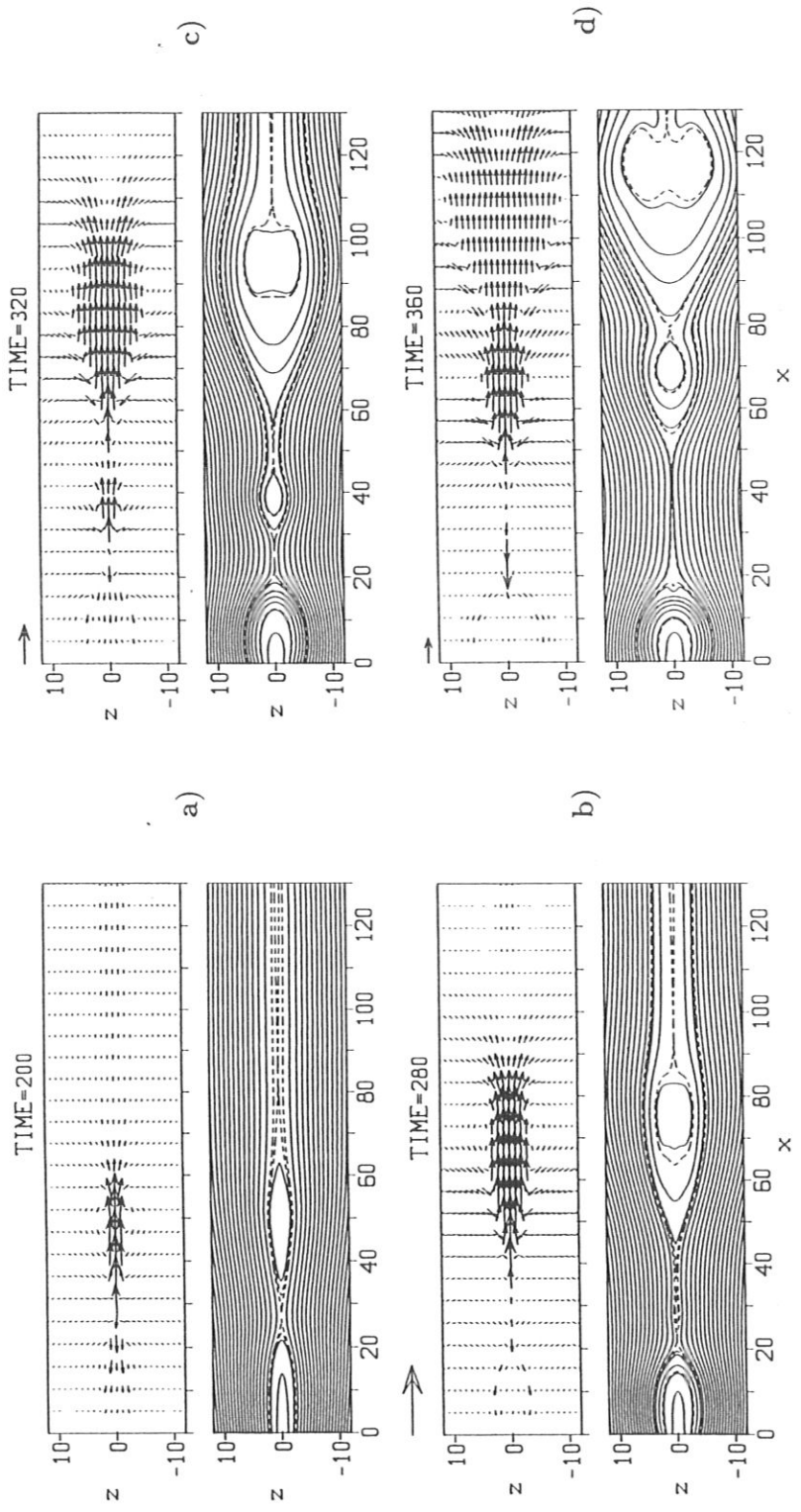

Figure 24: *Simulation of plasmoid generation in the geomagnetic tail. The arrows indicated above the charts of the flow pattern correspond to unit velocity (from Hautz and Scholer, 1987).*

Since the magnetotail plasma is collisionless, this has to be a collective process. Because of $T_i > T_e$, however, collisionless modes are in general strongly damped and cannot easily be excited which is consistent with the fact that the magnetotail is quiescent most of the time and substorms are rare events.

9 Magnetic reconnection in general three-dimensional systems

Up to this point consideration has been restricted to two dimensions, i.e. to systems with spatial symmetry, where the definition of magnetic reconnection in terms of a change of magnetic topology is unambiguous and the effect of reconnection is obvious by a simple inspection of the field configuration. Field line topology is determined by the flux function ψ with regions of different topology separated by separatrix surfaces ψ_s, connecting to X-type neutral points (or the generalizations thereof, such as osculating separatrices or current sheets with Y-points.

These concepts are, however, no longer valid in non-symmetric three-dimensional systems, which has led to certain misunderstandings. Following Schindler et al. (1988) we consider the process of plasmoid formation in a system of finite size in the z-direction with a superimposed weak B_z field, modelling the geomagnetic tail as illustrated in Fig. 25a. Obviously a separatrix, defined as a surface enclosing a region of field lines localized in x, does not exist, as all field lines finally connect to the left-hand tail edge. Nevertheless field line reconnection does occur in the sense of a localized break-down of the frozen-in field condition and a resulting change of the field line connection (this definition of reconnection has been given by Axford, 1984), as is illustrated in Fig. 25b. Hence in three-dimensional systems one has to resort to the original physical meaning of the term reconnection as localized magnetic diffusion, which implies the presence of a finite parallel electric field $E_{\|} = \eta j_{\|}$ (or some other dissipation effect in Ohm's law).

Since the simple two-dimensional criteria based on flux surface topology cannot be applied, it is interesting to obtain a more general criterion to decide whether in a given plasma volume V magnetic reconnection takes place. To this purpose one may use the magnetic helicity

$$H = \int_V \mathbf{A} \cdot \mathbf{B} \, d\tau \, .$$

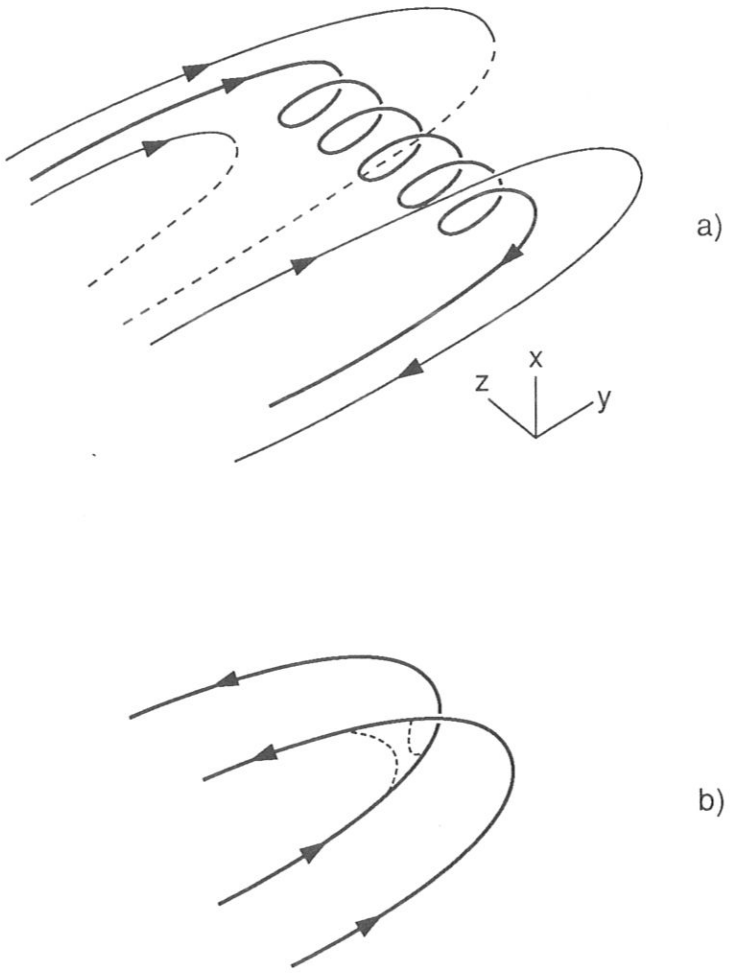

Figure 25: *(a) Schematic drawing of field lines in the geomagnetic tail with a finite component B_z, carrying a plasmoid.*
(b) Reconnection of two field lines in the process of plasmoid growth.

However, H is a useful quantity only if gauge invariant, which requires certain conditions on the surface S of the volume V to be satisfied. The time derivative of H is

$$\frac{dH}{dt} = -2\int_V \mathbf{E}\cdot\mathbf{B}\,d\tau - \oint_S (\phi\mathbf{B} + \mathbf{E}\times\mathbf{A})\cdot d\mathbf{F} \tag{86}$$

using $\partial_t\mathbf{B} = -\nabla\times\mathbf{E}$ and $\mathbf{E} = -\nabla\phi - \partial_t\mathbf{A}$. If $B_n = E_t = 0$ on the boundary, which corresponds to a conducting wall, the gauge-dependent surface term vanishes. In this case $dH/dt \neq 0$ indicates $E_{\|} \neq 0$ somewhere in the system, hence reconnection occurs. In astrophysical applications, however, the case of an unbounded system is of more interest, where dynamical processes are limited to a finite region, while outside there is a static magnetic field and no electric field. Here one can define a more general helicity expression

$$\overline{H} = \int_V (\mathbf{A} + \mathbf{A}_0)\cdot(\mathbf{B} - \mathbf{B}_0)\,d\tau\,, \tag{87}$$

where $\mathbf{B}_0$, $\mathbf{A}_0$ are field and vector potential at some reference time t_0. Analogously to eq. (86) one obtains

$$\frac{d\overline{H}}{dt} = -2\int_V \mathbf{E}\cdot\mathbf{B}\,d\tau + \oint_S [\phi\,(\mathbf{B} - \mathbf{B}_0) + \mathbf{E}\times(\mathbf{A} - \mathbf{A}_0)]\cdot d\mathbf{F}\,. \tag{88}$$

For a static asymptotic field $\mathbf{B} = \mathbf{B}_0$ and vanishing asymptotic electric field $\mathbf{E} = 0$ the surface integral vanishes. Hence $d\overline{H}/dt \neq 0$ implies $E_{\|} \neq 0$ and thus guarantees the presence of reconnection.

A different more explicit approach to the 3-D reconnection problem has been developed by Lau and Finn (1990). Given a regular magnetic field $\mathbf{B}(\mathbf{x}, t)$, how can one decide whether reconnection is involved and where the reconnection layers are located in space. Here reconnection is defined in the following way. The ideal form of Ohm's law $\mathbf{E}+\mathbf{v}\times\mathbf{B} = 0$ called the frozen-in condition implies a perpendicular plasma flow

$$\mathbf{v}_\perp = \mathbf{E}\times\mathbf{B}/B^2\,, \tag{89}$$

called the field line velocity. The electric field satisfies the condition $\mathbf{E}\cdot\mathbf{B} = 0$, from which follows the equation for the electrostatic potential

$$\mathbf{B}\cdot\nabla\phi = -\mathbf{B}\cdot\partial_t\mathbf{A}\,. \tag{90}$$

Only if a smooth solution ϕ exists in the volume considered, can the plasma flow be regular and ideal MHD valid throughout the volume. If ϕ exhibits

singularities, this implies a violation of the frozen-in condition. In this case magnetic reconnection is said to occur. Flow regularity requires, that in the vicinity of such ideal singularities the ideal Ohm's law is replaced by

$$\mathbf{E} + \mathbf{v} \times \mathbf{B} = \mathbf{R}\,,$$

where $\mathbf{R} = \eta\mathbf{j}$ or some equivalent process, hence $E_{\|} \neq 0$.

In two-dimensional systems singularities of $\phi(x, y)$ are located on the separatrix and in particular in the X-point. As an example consider the vector potential

$$\mathbf{A}(x, y, t) = -(\psi(x, y) + E_0 t)\mathbf{e}_z \tag{91}$$

with

$$\psi(x, y) = \frac{1}{2}(x^2 - y^2) \tag{92}$$

discussed in section 5, corresponding to the stationary magnetic field $\mathbf{B} = (B_x, B_y, B_z) = (y, x, B_0)$. Equation (90) becomes

$$\mathbf{B} \cdot \nabla\phi = B_0 E_0\,, \tag{93}$$

which has the solution

$$\phi = \frac{1}{2} B_0 E_0 \ln \left| \frac{x + y}{x - y} \right|\,, \tag{94}$$

essentially identical with eq. (40). Since in the present context ϕ is the electric potential, not the streamfunction of an incompressible flow (note that the field line velocity (89) is not assumed to be incompressible), the axial field B_0 appears in eq. (92). ϕ is singular on the separatrix $x = \pm y$, and hence reconnection occurs for any $E_0 \neq 0$. It is interesting to compute the field line velocity eq. (89)

$$\begin{aligned} \mathbf{v}_\perp &= \frac{(-\nabla\phi + E_0\mathbf{e}_z) \times (\mathbf{e}_z \times \nabla\psi + B_0\mathbf{e}_z)}{B^2} \\ &= \frac{B_0\mathbf{e}_z \times \nabla\phi - E_0\nabla\psi}{B^2} - \frac{\mathbf{e}_z \nabla\phi \cdot \nabla\psi}{B^2}\,. \end{aligned} \tag{95}$$

In this expression the first term is in the poloidal plane, the second in the axial direction. $\mathbf{v}_\perp$ can be expressed by two components v_1, v_2

$$\mathbf{v}_\perp = v_1 \nabla\psi / |\nabla\psi| + v_2 \left(\mathbf{B} \times \nabla\psi\right) / |\mathbf{B} \times \nabla\psi|\,,$$

where

$$
\begin{aligned}
v_1 &= \mathbf{v}_\perp \cdot \nabla\psi / |\nabla\psi| = -E_0 / \sqrt{x^2 + y^2} && (96)\\
v_2 &= \mathbf{v}_\perp \cdot (\mathbf{B} \times \nabla\psi) / |\mathbf{B} \times \nabla\psi| \\
&= \nabla\phi \cdot \nabla\psi / |\mathbf{B} \times \nabla\psi| \\
&= -2B_0 E_0 \, xy \Big/ \left[\left(x^2 - y^2\right) \sqrt{x^2 + y^2} \sqrt{B_0^2 + x^2 + y^2} \, \right] . && (97)
\end{aligned}
$$

The component v_1 describes the flow in the poloidal plane toward or away from the X-point. It represents the convection of the flux surfaces ψ, which is singular only at the X-point. The component v_2 describes the field line flow in the flux surface $\psi = const$ and has singularities along the separatrix surfaces $x = \pm y$. Only in the limit $B_0 = 0$ one has $v_2 = 0$. (Note that the field line velocity gives only the plasma motion $\mathbf{v}_\perp$ perpendicular to the field line. The parallel component has to be obtained from an additional equation determined by the plasma dynamics, for instance $\nabla \cdot \mathbf{v} = 0$ together with appropriate boundary conditions.)

Generalizing these concepts to three dimensions, a new feature arises, the existence of isolated nulls of the magnetic field, i.e. points, where $\mathbf{B} = 0$. Field nulls are structurally stable, meaning that they persist, when the system is weakly perturbed, their position being only slighty shifted, in contrast to the separatrix in a two-dimensional system, which vanishes, when the system becomes weakly three-dimensional. In the vicinity of a null (assumed to be located at $\mathbf{x} = 0$) the Taylor expansions of $\mathbf{B}$ and $\mathbf{j}$ are

$$
\begin{aligned}
B_i &= \beta_{ij} x_j && (98)\\
j_i &= \varepsilon_{ijk} \beta_{jk} \, . && (99)
\end{aligned}
$$

Because of $\nabla \cdot \mathbf{B} = 0$ the trace of the real matrix β_{ij} vanishes. The matrix has three eigenvalues, the properties of which are used for a classification of nulls (Fukao et al., 1975; Greene, 1988). If all eigenvalues are real, either one is positive and two negative (A-type) or two are positive and one negative (B-type), since their sum must vanish. The eigenvectors of the two eigenvalues of the same sign locally form a plane, which can be continued into a global surface Σ by following the field lines located in this plane. Following the field lines along the third eigenvector defines a curve γ in space. The field lines near an A-type null are shown in Fig. 26, the surface Σ_A dividing space into two regions not connected by field lines, and all field lines in one region converging to form a bundle around γ_A. A B-type null has the same

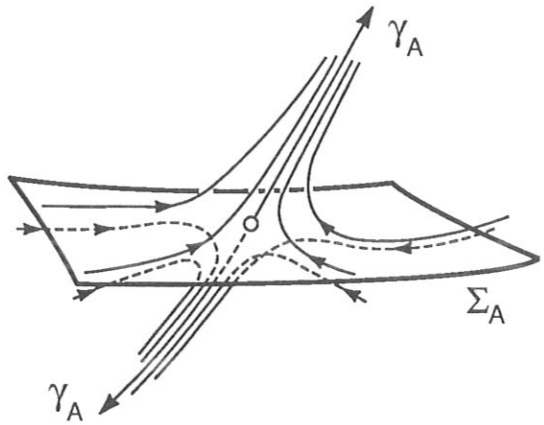

Figure 26: *Field lines near an A-type magnetic null.*

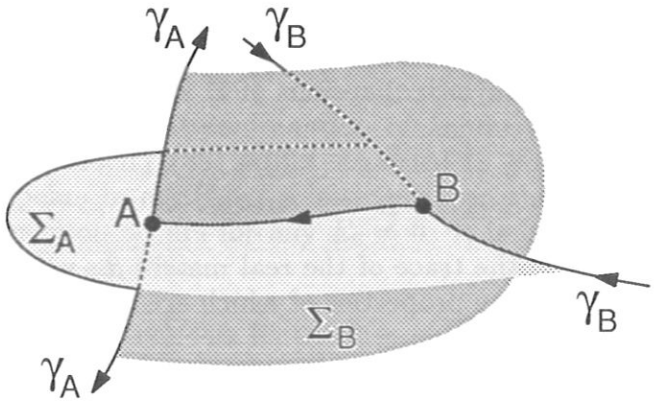

Figure 27: *Topology of a magnetic configuration including one A-type null (A) and one B-type null (B) (from Lau and Finn, 1990).*

topology with the field line directions reversed. A- or B-type nulls are the generalization of a two-dimensional X-point, into which they degenerate if one of the two eigenvalues of equal sign becomes zero. The correspondence to X-points can also be seen from the fact, that at A- or B-type nulls the current density (99) may vanish, since β_{ij} can be symmetric. These nulls are therefore expected to be important in the context of three-dimensional reconnection.

Nulls with one real and two conjugate complex eigenvalues (S-type) are generalizations of a two-dimensional O-point, to which they degenerate, if the real eigenvalue vanishes (in this case the remaining two are purely imaginary). As in the case of an O-point in the two-dimensional limit the current density cannot vanish at an S-type null, since β_{ij} is necessarily nonsymmetric.

A magnetic configuration with two nulls, one A-type and one B-type, is of special interest. The relative positions of the surfaces Σ_A, Σ_B and the curves γ_A, γ_B are illustrated in Fig. 27. Since in Σ_B all field lines are directed away from $\mathbf{B}$ and are collected in the bundle around γ_A, γ_A bounds Σ_B, and since all field lines in Σ_A must originate in the bundle around γ_B, γ_B bounds Σ_A. Hence Σ_A, Σ_B are semi-infinite half-sheets intersecting in a line connecting A and B, called a null-null line. A topologically equivalent configuration arises, when superimposing a constant field on a dipole field (e.g. the earth's magnetic field in the presence of an interplanetary field). Since the surfaces Σ_A, Σ_B are not pierced by field lines, they serve as separators, the three-dimensional generalization of the two-dimensional separatrix.

Lau and Finn calculated the field line velocity eq. (89) for a three-dimensional field configuration, consisting of the 2-D configuration eq. (92) periodically modulated in the z-direction. If the modulation is weak, such that B_z does not change sign, the behavior of $\mathbf{v}_\perp$ is qualitatively the same as in the unmodulated case. For sufficiently strong modulation B_z becomes zero at certain values of z and field nulls appear forming an alternating sequence of A- and B-type nulls. The singularities arising on the separatrix surfaces are of a more complicated type than in the case of no nulls and in addition essential singularities appears on the null-null lines between a pair of nulls.

This kinematic approach as developed by Lau and Finn (1990) is, however, only valid in the limit of vanishingly small reconnection rate $E_0 = O(\eta)$, since the effect of the singular flow dynamics on the magnetic field is neglected, $\mathbf{B}$ being prescribed as a smooth vector field. For larger values of E_0 the magnetic configuration is changed, presumably on a macroscopic scale.

In two dimensions Syrovatskii has shown that, whenever $E_0 \neq 0$ at an X-point, a current sheet of finite length appears, as discussed in section 4.3. The three-dimensional generalization in the presence of field nulls has still to be worked out.

Finally we consider three-dimensional toroidal configurations, where field lines are endless. Though field nulls do in general not occur, the new feature compared with the axisymmetric case is the appearance of regions of stochastic field line behavior. This means that such field lines are not localized to a particular flux surface but fill a finite volume. It appears that plasma flows resulting kinematically from the frozen-in condition $\mathbf{E} + \mathbf{v} \times \mathbf{B} = 0$ are singular in such a volume. Taking finite resistivity into account and allowing plasma dynamics to modify the field locally will probably lead to turbulent motions. MHD turbulence arising in regions of stochastic field lines has been invoked as a model for tokamak disruptions.

10 Turbulent reconnection

As stated at the beginning of this chapter, the fundamental problem in the theory of magnetic reconnection is to explain the observed fast times. In explosive magnetic processes such as tokamak disruptions or solar flares time scales seem to be essentially independent of the value of the collisional resistivity η, and primarily connected with typical Alfvén times $\tau_A = L/v_A$. Here L is the size of the region, where the magnetic field is affected, for instance the minor radius of a tokamak plasma or the length of a magnetic loop or arcade in the solar atmosphere.

As a consequence stationary current sheet reconnection, which appears to be the dominant mechanism for intermediate values of S, becomes too slow for "realistic" S-values. A possible solution of the problem is to consider further nonideal effects in Ohm's law such as (anomalous) electron viscosity or electron inertia, which in a weakly collisional plasma may be more important than resistivity. However, a more effective modification of the reconnection process at smaller η seems to be caused by a nonstationary behavior in the reconnection region. A first indication of such behavior is provided by the occasional generation and ejection of plasmoids. If η is further decreased, plasmoids are generated more frequently and in a more irregular way, with plasmoid coalescence becoming an important reconnection process, as seen in Fig. 24. Thus secondary small current sheets are generated with life times small compared to the global reconnection time. It is not difficult to visu-

alize a gradual transition to a state of fully developed MHD turbulence, in particular for nonsymmetric systems. In a region of stochastic field lines in a toroidal plasma a certain level of small-scale turbulence is expected even under macroscopically quiescent conditions.

Turbulent dissipation in MHD systems is very efficient, with energy dissipation rates becoming essentially independent of η for large Reynolds numbers already in two dimensions, in contrast to 2-D Navier-Stokes turbulence (Biskamp and Welter, 1989). This property is the more true in three dimensions. In a reconnecting system turbulence is not spread uniformly over the entire magnetic configuration but predominantly confined to regions of relatively small extent, where it is excited by strong field gradients, i.e. high current density. The regions of strong turbulence are probably not fixed in space but expected to fluctuate appearing here and there which gives rise to an burst-like global behavior.

Small-scale MHD turbulence gives rise to a turbulent resistivity η_{eff} and hence to an effective reconnection rate independent of the value of the collisional resistivity η. An explicit expression for η_{eff} in terms of the fluctution amplitudes $\delta\mathbf{B}$, $\delta\mathbf{v}$ has only been derived under special assumptions (see for instance Biskamp, 1984). The fact that turbulence is mainly excited in regions of high current density suggests a linear relation

$$\eta_{eff} = \eta + \alpha(j - j_0)\,, \tag{100}$$

where j_0 is some threshold value. Such relation is often used as a simple anomalous resistivity model (e.g. Sato and Hayashi, 1979). Note that this expression is motivated by properties of MHD turbulence and hence remains within the framework of MHD theory, so that no ad hoc assumption about the excitation of current-driven micro-instabilities is required, though the latter can of course also contribute to η_{eff}.

The arbitrariness in using expression (100) is above all connected with the choice of the threshold value j_0. Consider the process of island coalescence, section 8.1, in the limit of $\eta \to O_+$, where a unique η-independent turbulent behavior is to be expected. If in modeling this process j_0 is assumed to be rather low, the resulting process resembles the reconnection by a quasi-stationary current sheet at relatively high η. Choosing a somewhat higher value of j_0 would allow the system to develop nonstationary features, connected with plasmoid generation, but still suppress further fine-scale effects. Hence the value of j_0 determines the level up to which the reconnection

dynamics is resolved. The question, to what extent a low-level model using a simple relation such as (100) can describe the global features of the full turbulent ($\eta \to O_+$) system, is difficult to answer.

Though a quantitative theory of turbulent reconnection is certainly very complicated, the existence of turbulent dissipation rates independent of η in principle solves the problem of explaining sufficiently fast reconnection time scales, a problem which in retrospective arises only when extrapolating stationary current sheet reconnection rates to the limit of small η. However, for practical applications with a given low level of collisionality the general statement that reconnection becomes independent of η for sufficiently small values is often not very helpful, and even misleading. An example is given by the sawtooth collapse in a hot tokamak plasma. Though typical S-values appear to be very large, $S \sim 10^8$, experiments indicate that reconnection is considerably slower than the temperature collapse time scale, since little helical flux appears to be reconnected.

References

[1] Ara, G., Basu, B., Coppi, B., Laval, G., Rosenbluth, M.N., and Waddell, B.V. (1978). Magnetic reconnection and $m = 1$ oscillation in current carrying plasmas, *Ann. Phys.* **112**, 443–476.

[2] Axford, W.I. (1984). Magnetic reconnection, in *Magnetic Reconnection in Space and Laboratory Plasmas, Geophys. Monogr. Ser.*, vol. **30**, ed. E.W. Hones, Jr., pp. 1–8 (AGU, Washington, DC).

[3] Birn, J., and Hones, Jr., E.W. (1981). Three-dimensional computer modeling of dynamic reconnection in the geomagnetic tail, *J. Geophys. Res.* **86**, 6802–6808.

[4] Biskamp, D. (1984). Anomalous resistivity and viscosity due to small scale magnetic turbulence, *Plasma Phys. Contr. Fusion* **26**, 311–319.

[5] Biskamp, D. (1986). Magnetic reconnection via current sheets, *Phys. Fluids* **29**, 1520–1531.

[6] Biskamp, D. (1991). Algebraic nonlinear growth of the resistive kink instability, to appear in *Phys. Fluids* **B3**.

[7] Biskamp, D., and Welter, H. (1980). Coalescence of magnetic islands, *Phys. Rev. Lett.* **44**, 1069–1072.

[8] Biskamp, D., and Welter, H. (1989). Dynamics of decaying two-dimensional magnetohydrodynamic turbulence, *Phys. Fluids* **B1**, 1964–1979.

[9] Bulanov, S.V., Sakai, J., and Syrovatskii, S.I. (1979). Tearing mode instability in approximately steady MHD configurations, *Sov. J. Plasma Phys.* **5**, 157–163.

[10] Cowley, S.W.H. (1975). Magnetic field line reconnection in a highly-conducting incompressible fluid: properties of the diffusion region, *J. Plasma Phys.* **14**, 475–490.

[11] Fadeev, V.M., Kvartskhava, I.F., and Komarov, N.N. (1965). Self-focusing of local plasma currents, *Nucl. Fusion* **5**, 202–209.

[12] Finn, J.M., and Kaw, P.K. (1977). Coalescence instability of magnetic islands, *Phys. Fluids* **20**, 72–78.

[13] Forbes, T.G., and Priest, E.R. (1987). A comparison of analytical and numerical models for steadily driven magnetic reconnection, *Rev. Geophys.* **25**, 1587–1607.

[14] Fukao, S., Masayuki, U., and Takao, T. (1975). Topological study of magnetic field near a neutral point, *Rep. Ionosph. Res. Jpn.* **29**, 133–139.

[15] Furth, H.P., Killeen J., and Rosenbluth, M.N. (1963). Finite resistivity instabilities of a sheet pinch, *Phys. Fluids* **6**, 459–484.

[16] Greene, J.M. (1988). Geometrical properties of three-dimensional reconnecting magnetic fields with nulls, *J. Geophys. Res.* **93**, 8583–8590.

[17] Hautz, R., and Scholer, M. (1987). Numerical simulation on the structure of plasmoids in the deep tail, *Geophys. Res. Lett.* **14**, 969–972.

[18] Kadomtsev, B.B., and Pogutse, O.P. (1974). Nonlinear helical perturbations of a plasma in the tokamak, *Sov. Phys.-JETP* **38**, 283–290.

[19] Kageyama, A., Watanabe, K., and Sato, T. (1990). Global simulation of the magnetosphere with a long tail: The formation and ejection of plasmoids, National Institute of Fusion Studies, Res. Report NIFS-49, Nagoya, Japan.

[20] Lau, Y.T., and Finn, J.M. (1990). Three-dimensional kinematic reconnection in the presence of field line nulls and closed field lines, *Astrophys. J.* **350**, 672–691.

[21] Lee, L.C., Fu, Z.F., and Akasofu, S.I. (1985). A simulation study of forced reconnection processes and magnetospheric storms and substorms, *J. Geophys. Res.* **90**, 10896–10910.

[22] Otto, A., Schindler, K., and Birn, J. (1990). Quantitative study of the nonlinear formation and acceleration of plasmoids in the earth's magnetotail, *J. Geophys. Res.* **95**, 15023–15037.

[23] Park, W., Monticello, D.A., and White, R.B. (1984). Reconnection rates of magnetic fields including the effects of viscosity, *Phys. Fluids* **27**, 137–149.

[24] Parker, E.N. (1963). The solar flare phenomenon and the theory of reconnection and annihilation of magnetic fields, *Astrophys. J. Suppl.* Ser. **8**, 177–211.

[25] Petschek, H.E. (1964). Magnetic field annihilation, in *AAS/NASA Symposium on the Physics of Solar Flares*, ed. W.N. Hess (NASA, Washington, DC), 425–437.

[26] Priest, E.R., and Forbes, T.G. (1986). New models for fast steady state magnetic reconnection, *J. Geophys. Res.* **91**, 5579–5588.

[27] Pritchett, P.L., and Wu, C.C. (1979). Coalescence of magnetic islands, *Phys. Fluids* **22**, 2140–2146.

[28] Rutherford, P.H. (1973). Nonlinear growth of the tearing mode, *Phys. Fluids* **16**, 1903–1908.

[29] Sato, T., and Hayashi, T. (1979). Externally driven magnetic reconnection and a powerful magnetic energy converter, *Phys. Fluids* **22**, 1189–1202.

[30] Schindler, K., Hesse, M., and Birn, J. (1988). General magnetic reconnection, parallel electric fields, and helicity, *J. Geophys. Res.* **93**, 5547–5557.

[31] Shivamoggi, B.K. (1985). Magnetohydrodynamic properties near an X-type magnetic neutral line, *J. Plasma Phys.* **31**, 333–335.

[32] Sonnerup, B.U. (1970). Magnetic field reconnection in a highly conducting incompressible fluid, *J. Plasma Phys.* **4**, 161–174.

[33] Strauss, H.R. (1976). Nonlinear three-dimensional magnetohydrodynamics of noncircular tokamaks, *Phys. Fluids* **19**, 134–140.

[34] Sweet, P.A. (1958). The production of high energy particles in solar flares, *Nuovo Cimento Suppl.* **8**, *Ser. X*, 188–196.

[35] Syrovatskii, S.I. (1971). Formation of current sheets in a plasma with a frozen-in strong magnetic field, *Sov. Phys. JETP* **33**, 933–940.

[36] Syrovatskii, S.I. (1981). Pinch sheets and reconnection in astrophysics, *Ann. Rev. Astron. Astrophys.* **19**, 163–229.

[37] Ugai, M. (1989). Computer studies of a large-scale plasmoid driven by spontaneous fast reconnection, *Phys. Fluids* **B1**, 942–948.

[38] Vasyliunas, V.M. (1975). Theoretical models of magnetic field line merging, *Rev. Geophys. Space Phys.* **13**, 303–336.

[39] Waelbroeck, F.L. (1989). Current sheets and nonlinear growth of the $m = 1$ kink-tearing mode, *Phys. Fluids* **B1**, 2372–2380.

[40] Yeh, T., and Axford, W.I. (1970). On the reconnection of magnetic field lines in conducting fluids, *J. Plasma Phys.* **4**, 207–229.